Hindawi Publishing Corporation
Journal of Applied Mathematics
Volume 2012, Article ID 938727, 26 pages
doi:10.1155/2012/938727

Research Article

Adaptive Double-Diffusion Model and Comparison to a Highly Heterogeneous Micro-Model

Viviane Klein[1] and Malgorzata Peszynska[2]

[1] *Campus Araranguá, Universidade Federal de Santa Catarina, Rua Pedro João Pereira, 150, 88900-000 Araranguá, SC, Brazil*
[2] *Department of Mathematics, Oregon State University, 368 Kidder Hall, Corvallis, Oregon 97331-4605, USA*

Correspondence should be addressed to Viviane Klein, viviane.klein@ufsc.br

Received 21 March 2012; Accepted 13 April 2012

Academic Editor: Khalida Inayat Noor

Copyright © 2012 V. Klein and M. Peszynska. This is an open access article distributed under the Creative Commons Attribution License, which permits unrestricted use, distribution, and reproduction in any medium, provided the original work is properly cited.

Double-diffusion model is used to simulate slightly compressible fluid flow in periodic porous media as a macro-model in place of the original highly heterogeneous micro-model. In this paper, we formulate an adaptive two-grid numerical finite element discretization of the double-diffusion system and perform a comparison between the micro- and macro-model. Our numerical results show that the micro-model solutions appear to converge to the macro-model linearly with the parameter ε of periodic geometry. For the two-grid discretization, the a priori and a posteriori error estimates are proved, and we show how to adapt the grid for each component independently.

1. Introduction

When modeling phenomena in highly heterogeneous media, one frequently finds that the coefficients of differential equations describing these phenomena vary by several orders of magnitude between close-by locations. Consequently, the solutions to the exact, that is, *micro*-models, vary at multiple separate spatial and time scales, and it is convenient to work with their spatial and temporal averages, that is, with the solutions to *macro*-models. Various multiscale modeling techniques have been introduced with the aim to derive, analyze, and approximate micro-models by the macro-models. In particular, the mathematical framework for construction and analysis of the average, that is, *homogenized*, models for *multiscale* media is well understood, see, for example, [1–3]. However, there are few results devoted to the comparison between the micro- and macro-models for evolution equations and to their adaptive numerical discretizations.

Consider the following transient diffusion model which describes the density ρ of single-phase slightly compressible flow in a porous domain Ω:

$$\phi \frac{\partial \rho}{\partial t} - \nabla \cdot (k \nabla \rho) = f, \quad \text{in } \Omega, t > 0, \tag{1.1}$$

where the coefficients ϕ, k denote, respectively, the porosity and conductivity.

In this paper, we propose a two-grid adaptive finite element approximation of the following multiscale averaged model for (1.1) in highly heterogeneous media such as porous media with fractures

$$\widetilde{\phi}_1 \frac{\partial \widetilde{\rho}_1}{\partial t} - \nabla \cdot \left(\widetilde{k}_1 \nabla \widetilde{\rho}_1 \right) + c(\widetilde{\rho}_1 - \widetilde{\rho}_2) = \widetilde{f}, \quad \text{in } \Omega, t > 0, \tag{1.2a}$$

$$\widetilde{\phi}_2 \frac{\partial \widetilde{\rho}_2}{\partial t} - \nabla \cdot \left(\widetilde{k}_2 \nabla \widetilde{\rho}_2 \right) + c(\widetilde{\rho}_2 - \widetilde{\rho}_1) = 0, \quad \text{in } \Omega, t > 0, \tag{1.2b}$$

proposed in [4, 5]. The system (1.2a) and (1.2b) describes the average behavior of fluids in media with two or more subregions of distinct features, where the subregions may or may not be connected globally at micro-scale. At macro-scale the interaction of fluids associated with these subregions is modeled with the *exchange term* $c(\widetilde{\rho}_2 - \widetilde{\rho}_1)$, and the coefficients $\widetilde{k}_i$, $\widetilde{\phi}_i$ are computed from micro-scale geometry and coefficients. The system (1.2a) and (1.2b) is useful in applications in porous media as well as in description of other multiscale evolution phenomena in heterogeneous media, for example, heat conduction. In addition, its special, degenerate, case of (1.2a) and (1.2b) with $\widetilde{k}_2 = 0$ known as the Warren-Root model [6]

$$\widetilde{\phi}_1 \frac{\partial \widetilde{\rho}_1}{\partial t} - \nabla \cdot \left(\widetilde{k}_1 \nabla \widetilde{\rho}_1 \right) + c(\widetilde{\rho}_1 - \widetilde{\rho}_2) = \widetilde{f}, \quad \text{in } \Omega, t > 0, \tag{1.3a}$$

$$\widetilde{\phi}_2 \frac{\partial \widetilde{\rho}_2}{\partial t} + c(\widetilde{\rho}_2 - \widetilde{\rho}_1) = 0, \quad \text{in } \Omega, t > 0, \tag{1.3b}$$

is a popular way of modeling of subscale diffusion accompanying advection and adsorption, see [7–10].

The macro-model (1.2a) and (1.2b) of interest to this paper was introduced in [4] based on heuristic arguments. The model, while intuitively clear and useful for practical purposes, for a long time was lacking a rigorous multiscale analysis and interpretation via an associated appropriate micro-model. Only recently in [11] it was shown rigorously by two-scale convergence that (1.2a) and (1.2b) is indeed a homogenized limit of (1.1) in certain highly heterogeneous media. Most interesting is that the original microstructure which leads to (1.2a) and (1.2b) is composed of *three* rather than *two* media as in [12]. Also, the derivation in [11] demonstrates clearly that in two-dimensional geometries and more generally for quasistatic models in disconnected microscale subregions we have $\widetilde{k}_2 = 0$.

However, the analysis in [11] does not include a direct comparison of (1.1) and (1.2a) and (1.2b), and this motivated our research. We compare the computational solutions to (1.2a) and (1.2b) and (1.1) quantitatively in function of the microstructure parameters. In

addition, since typically $0 \le \tilde{k}_2 \ll \tilde{k}_1$, it is natural to suggest that in numerical simulation $\tilde{\rho}_1$ and $\tilde{\rho}_2$ should be approximated on separate grids, since they evolve differently and since this can lead to more efficient numerical algorithms. In fact, the spatial grids should be chosen adaptively guided by some a posteriori estimators and should be allowed to vary in time. The idea of using two grids extends that in [13] where we considered a stationary analogue of (1.2a) and (1.2b) and proved upper and lower bounds for residual type a posteriori estimators. The estimators proposed in [13] were shown to be *robust*, that is, insensitive to $\tilde{k}_2 \approx 0$ and to other parameters. In this paper we extend those to the evolution system (1.2a) and (1.2b) and present an a posteriori error estimator of residual type based partly on the work in [14–16] for scalar equations.

The aim of this paper is thus twofold, and the paper is organized as follows. In Section 2 we introduce the notation and the generic flow model as well as its numerical approximation. In Section 3 we develop the details of micro- and macro- models and compare their discrete solutions in function of a characteristic parameter of the microstructure ε. In Section 4, we define the numerical approximations to these models and formulate the *a-priori* and *a-posteriori* estimates for the approximation error. We then illustrate the use of *a-posteriori* estimators with an adaptive example. The appendix provides the technical proofs of some of the results derived in this paper.

2. Notation and Preliminaries on the Flow Model

Here we introduce the notation and preliminaries. We follow, for example, [17, 18]. Let the domain of flow $\Omega \subset \mathbb{R}^d$, $d = 2, 3$, be a bounded polygonal region with piecewise smooth boundary $\partial\Omega = \overline{\Gamma_D \cup \Gamma_N}$, where Γ_D, Γ_N are disjoint regions of the boundary $\partial\Omega$ where Dirichlet and Neumann boundary conditions are prescribed, respectively.

For any subset $\omega \subseteq \Omega$, we use the standard notation for Lebesgue $L^2(\omega)$ and Sobolev spaces $H^k(\omega)$, $k \in \mathbb{N}$. These are equipped with the usual seminorms $|\cdot|_{k,\omega}$, norms $\|\cdot\|_{k,\omega} := \|\cdot\|_{H^k(\omega)}$ and the usual scalar product (s) $(f,g)_\omega := (f,g)_{L^2(\omega)}$. We denote $\|f\|_\omega := (f,f)_\omega^{1/2}$. If $\omega = \Omega$, the subscript ω will be omitted. We also let $H^1_D(\Omega) := \{v \in H^1(\Omega) : v|_{\Gamma_D} = 0\}$ under the standard norm in $H^1(\Omega)$, $\|v\|_1 := (\|v\|^2 + \|\nabla v\|^2)^{1/2}$.

For any $T > 0$ and any vector space S, the space $L^2(0,T;S)$ consists of all square-integrable functions with values in S such that $\|v\|_{L^2(0,T;S)} := (\int_0^T \|v\|_S^2)^{1/2}$ is finite. The space $C([0,T];S)$ is defined similarly.

2.1. Variational Form of Micro-Model

Consider (1.1) as a model for single-phase slightly compressible flow in porous media in which the gravity terms have been ignored; see [19] for derivation. Here $\phi = \phi(x)$ and $k = k(x)$, $x \in \Omega$ denote the nonnegative coefficients of porosity and conductivities, respectively, and f accounts for external sources. We assume for simplicity that k is a scalar quantity.

It is well known that (1.1) is well posed if appropriate boundary and initial data are imposed. We will use

$$\begin{aligned} \rho &= \rho_0, \quad \text{in } \Omega \times \{0\}, \\ \rho &= \rho_D, \quad \text{on } \Gamma_D, \\ k\nabla\rho \cdot \vec{n} &= 0, \quad \text{on } \Gamma_N. \end{aligned} \tag{2.1}$$

For simplicity we assume that $\rho_D \equiv 0$ and that the flow is driven by f. However, in simulation examples we use $f \equiv 0$, $\rho_D \not\equiv 0$.

The variational formulation of problem (1.1) and (2.1) reads

Find $\rho \in C([0,T]; L^2(\Omega)) \cap L^2(0,T; H_D^1(\Omega))$ *so that*

$$\left(\phi \frac{\partial \rho}{\partial t}, \psi\right) + (k\nabla\rho, \psi) = (f, \psi), \quad \forall \psi \in H_D^1(\Omega). \tag{2.2}$$

For any $\rho_0 \in L^2(\Omega)$, $f \in C([0,T]; L^2(\Omega))$, there is a unique solution $\rho \in C([0,T]; L^2(\Omega)) \cap L^2(0,T; H_D^1(\Omega))$ to (2.7); see [20, Theorem 11.1.1, page 366]).

2.2. Variational Form of Macro-Model

Now consider (1.2a) and (1.2b) and assume that $\tilde{\phi}_1$, $\tilde{\phi}_2$, $\tilde{k}_1$, $\tilde{k}_2$, and $c \in L^\infty(\Omega)$ are bounded uniformly from above and below by positive constants and are independent of time. We consider separately the particular case of (1.3a) and (1.3b) when $\tilde{k}_2 \equiv 0$.

Our variational formulation for (1.2a) and (1.2b) uses the theory developed in [17, 18] for evolution problems with m-accretive operators by the Hille-Yosida Theorem. For analysis of classical solutions see [21, 22].

For the macro-model (1.2a) and (1.2b) and if $\tilde{k}_2 > 0$, we assume the following initial and boundary conditions defined for $i = 1, 2$:

$$\begin{aligned} \tilde{\rho}_i &= \tilde{\rho}_{i,0}, \quad \text{in } \Omega \times \{0\}, \\ \tilde{\rho}_i &= \rho_D, \quad \text{on } \Gamma_D, \\ \tilde{k}_i \nabla \tilde{\rho}_i \cdot \vec{n} &= 0, \quad \text{on } \Gamma_N. \end{aligned} \tag{2.3}$$

As before, we assume that $\rho_D \equiv 0$ for now.

Let $\tilde{\rho}_i(\cdot, 0) = \tilde{\rho}_{i,0} \in L^2(\Omega)$, $f \in C([0,T], L^2(\Omega))$, $u_D \equiv 0$. The variational form of (1.2a), (1.2b), and (2.3) is as follows:

Find $\tilde{\rho}_i \in C([0,T]; L^2(\Omega)) \cap L^2(0,T; H_D^1(\Omega))$, $i = 1, 2$, *such that*

$$\begin{aligned} \left(\tilde{\phi}_1 \frac{\partial \tilde{\rho}_1}{\partial t}, \psi\right) + \left(\tilde{k}_1 \nabla \tilde{\rho}_1, \nabla \psi\right) + \left(c(\tilde{\rho}_1 - \tilde{\rho}_2), \psi\right) &= (f, \psi), \quad \forall \psi \in H_D^1(\Omega), \\ \left(\tilde{\phi}_2 \frac{\partial \tilde{\rho}_2}{\partial t}, \xi\right) + \left(\tilde{k}_2 \nabla \tilde{\rho}_2, \nabla \xi\right) + \left(c(\tilde{\rho}_2 - \tilde{\rho}_1), \xi\right) &= 0, \quad \forall \xi \in H_D^1(\Omega). \end{aligned} \tag{2.4}$$

The well posedness of this system (2.4) follows immediately by showing that the operator $\mathcal{B} : \mathfrak{D} \subset H_D^1(\Omega) \times H_D^1(\Omega) \to L^2(\Omega) \times L^2(\Omega)$

$$\mathcal{B} = \begin{bmatrix} -\partial \tilde{k}_1 \partial + cI & -cI \\ -cI & -\partial \tilde{k}_2 \partial + cI \end{bmatrix}, \text{ where } I \text{ is the identity operator,} \tag{2.5}$$

is m-accretive. The accretiveness is straightforward by showing that $(Bu, u) \geq 0$ in the product space. The maximal property follows from that of the operators $-\partial\widetilde{k}_i\partial$, I.

Now, if $\widetilde{k}_2 \equiv 0$, we do not impose boundary conditions on $\widetilde{\rho}_2$. The variational formulation of (3) and (2.3), reads

Find $\widetilde{\rho}_1 \in C([0,T]; L^2(\Omega)) \cap L^2(0,T; H^1_D(\Omega))$, $\widetilde{\rho}_2 \in C([0,T]; L^2(\Omega)) \cap L^2(0,T; L^2(\Omega))$ *such that*

$$\begin{gathered}\left(\widetilde{\phi}_1 \frac{\partial \widetilde{\rho}_1}{\partial t}, \psi\right) + \left(\widetilde{k}_1 \nabla \widetilde{\rho}_1, \nabla \psi\right) + \left(c(\widetilde{\rho}_1 - \widetilde{\rho}_2), \psi\right) = (f, \psi), \quad \forall \psi \in H^1_D(\Omega), \\ \left(\widetilde{\phi}_2 \frac{\partial \widetilde{\rho}_2}{\partial t}, \xi\right) + \left(c(\widetilde{\rho}_2 - \widetilde{\rho}_1), \xi\right) = 0, \quad \forall \xi \in L^2(\Omega).\end{gathered} \tag{2.6}$$

The well posedness of (2.6) follows similarly from the Hille-Yosida theorem. Also, $\widetilde{\rho}_2$ has the minimum of regularity of its initial data and of $\widetilde{\rho}_1$.

2.3. Notation on Numerical Discretization

For computations of solutions we use conforming (Galerkin) finite elements for spatial discretization and implicit Euler time stepping. We partition the time interval $[0,T]$ into subintervals $[t_{n-1}, t_n]$, $1 \leq n \leq N$, such that $0 = t_0 < t_1 < \cdots < t_N = T$. We denote $\Delta t_n = t_n - t_{n-1}$ and $z(t_n) = z^n$ for any function z.

For spatial discretization, we adopt standard finite element nomenclature that can be found in textbooks such as [23–25]. At each time step n, we denote by $\mathcal{T}_h^n$, $h > 0$, a family of admissible and shape-regular partitions of Ω into a finite number of elements. For any element $T \in \mathcal{T}_h^n$, we let h_T be the diameter of T and denote $h = \max_{T\in\mathcal{T}_h} h_T$. Also, $\mathcal{E}_h^n$ is the set of all edges of $\mathcal{T}_h^n$. For any edge $E \in \mathcal{E}_h^n$, we let h_E denote the diameter of the edge E. Finally, we denote by $\mathcal{P}_k(T)$ the space of polynomials of degree k in $\mathbb{R}^d$.

Numerical Approximation of Micro-Model

At each time step n, we define

$$V_h^n = \left\{ v_h \in C\left(\overline{\Omega}\right) : \forall T \in \mathcal{T}_h^n,\ v_h|_T \in \mathcal{P}_k(T),\ v|_{\Gamma_D} = 0 \right\}, \tag{2.7}$$

and seek an approximation $\rho_h^n \in V_h^n$ such that for all $\psi_h \in V_h^n$

$$\left(\phi \frac{\rho_h^n - \rho_h^{n-1}}{\Delta t_n}, \psi_h\right) + \left(k \nabla \rho_h^n, \nabla \psi_h\right) = (f, \psi_h), \tag{2.8a}$$

$$\rho_h^0 = \mathcal{I}_h \rho_0 \quad \text{in } \Omega. \tag{2.8b}$$

Here $\mathcal{I}_h$ denotes an interpolation or projection operator into V_h^n.

It is standard [20] that there is a unique solution $\rho_h^n \in V_h^n$ for (2.8a) at each n, $1 \leq n \leq N$. A priori estimates for the error between the solution to (2.2) and that of (2.8a) and (2.8b) can be found in the literature, see, for example, [20, 25, 26]. For a posteriori error estimates for

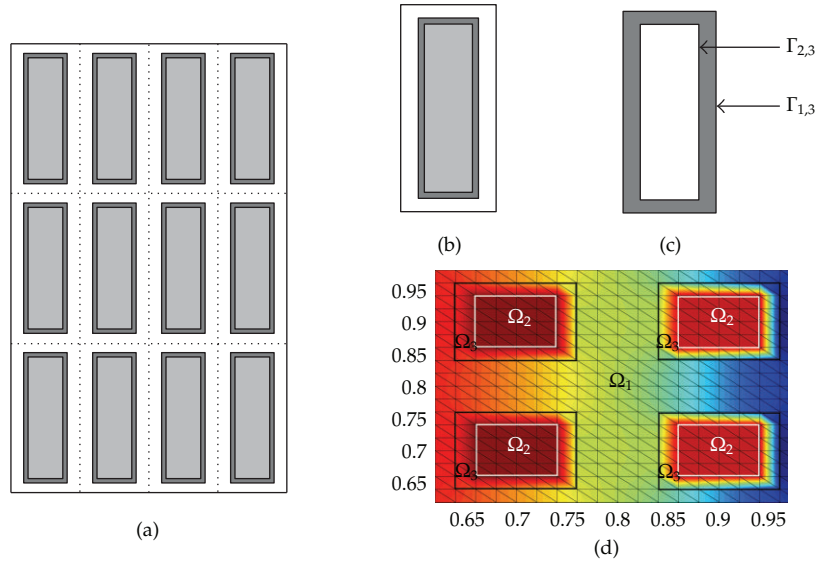

Figure 1: Periodic heterogeneous media. (a) Ω_1: white, Ω_2: grey, and Ω_3: dark grey. (b) Zoom of one cell Y: Y_1: white, Y_2: grey, and Y_3: dark grey. (c) Y_3 in grey with the internal and external boundaries $\Gamma_{2,3}$, $\Gamma_{1,3}$, respectively. (d) Illustration of three regions as in Example 3.1, where Ω_2 is delimited by the white boundaries, and Ω_3 is the region between by the black and the white boundaries.

parabolic problems see [15, 27–29]; the methods in the latter two papers are most relevant to our paper.

Numerical Approximation of Macro-Model

Consider now a fully discrete approximation to the solutions to (2.4) or (2.6). The formulation with a fixed grid immediately extends (2.8a) and (2.8b), and appropriate error estimates can be proven. More generally, each of $\tilde{\rho}_i$ can be associated with its own grid $\mathcal{T}_{h_i}^n$; see details in Section 4.

3. Comparison of Micro- and Macro-Models

The difficulties associated with numerical approximation (2.8a) and (2.8b) to (1.1) arise when ϕ, k are highly varying coefficients. In particular, consider a porous domain Ω composed of three disjoint regions Ω_i, $i = 1, \ldots, 3$, see Figure 1, with positive constants $(\phi_i, k_i)_{i=1}^3$ so that

$$\begin{aligned} \phi(x) &= \phi_1\chi_1(x) + \phi_2\chi_2(x) + \phi_3\chi_3(x), \\ k(x) &= k_1\chi_1(x) + k_2\chi_2(x) + k_3\chi_3(x). \end{aligned} \tag{3.1}$$

Here χ_i denotes the characteristic function of Ω_i.

An accurate numerical approximation to (1.1) with (3.1) requires that the grid $\mathcal{T}_h$ is very fine so that it lines up with the interfaces $\partial\Omega_i \cap \partial\Omega_k$. The computational complexity of the associated numerical implementation is very large whenever the geometry of interfaces is complex, but this can be overcome by a modeling approximation. In [11] it is shown that

(1.2a) and (1.2b) provides solutions close to those of (1.1), with the coefficients $\widetilde{\phi}_i, \widetilde{k}_i$ which do not vary locally. Thus a grid for (1.2a) and (1.2b) can be chosen depending on the global macrodynamics rather than local microdynamics and, consequently, it can be much coarser than $\mathcal{T}_h$.

3.1. Derivation of Macro-Model

One successful avenue to reduce the complexity of a highly heterogeneous model is to consider a *homogenized* or *upscaled* problem, whose coefficients are derived from the original coefficients [1, 2, 30], and which can be simulated on a coarse grid quite accurately. However, for time-dependent problems, this leads to inaccurate representation of the global dynamics, especially if $k_1 \gg k_2$ and/or $k_1 \gg k_3$.

The *double-diffusion* models proposed in [4], the *relaxation* model from [6], and *double-porosity models* derived in [12] are families of successful modeling strategies for parabolic PDEs with periodic highly heterogeneous media. The recent general derivation in [11] is most general and includes those from [4, 6, 12] as special cases.

The double-diffusion model developed in [4] was shown in [11] to be a limit of a certain micro-model with three regions arranged periodically. The rigorous derivation in [11] allows for each of the regions Ω_i to be connected. Furthermore, it assumes that Ω_3 separates Ω_1 and Ω_2, that is, that $\partial\Omega_1 \cap \partial\Omega_2 = \emptyset$. The model in [11] develops a general nonlocal exchange term acting across Ω_3. Its special case equivalent to the model in [4] assumes $\phi_3 \approx 0$ thereby making a *quasistatic* assumption and allows to compute the coefficient c explicitly.

Double-porosity models proposed in [12] assume that only one of the regions Ω_1 is connected and so effectively one can set $\Omega_2 = \emptyset$. However, $\phi_3 > 0$. In the macro-model the second equation (1.2b) is replaced by a local micro-model equation, the exchange follows through macro-micro boundary conditions and is nonlocal in nature. We refer to [31–35] for various analyses, models, approximations, and extensions of double-porosity models.

Of course, all three regions Ω_1, Ω_2, and Ω_3 can be connected only in $d = 3$. In $d = 2$ only one of these regions, say Ω_1, can be connected; see Figure 1(a). As we point out below, this implies $\widetilde{k}_2 = 0$, and the macro-model (1.2a) and (1.2b) in $d = 2$ becomes the Warren-Root relaxation model (3) as in [6].

In this paper we are interested in the double-diffusion models with a constant c from [4, 6] and its corresponding quasistatic micro-model from [11]. The exchange region Ω_3 is assumed to be small and acts like a thick skin separating Ω_1 from Ω_2. In consequence, the fluid flows effectively only in two regions Ω_1 and Ω_2; this is represented by the two sub-equations in (1.2a) and (1.2b). Details, comparison, and simulations are shown in what follows.

3.1.1. Macro-Model Parameters

To compute parameters $\widetilde{\phi}_1$, $\widetilde{\phi}_2$, $\widetilde{k}_1$, $\widetilde{k}_2$, and c of the macro-model (1.2a) and (1.2b), one has to calculate local averages and compute auxiliary solutions of differential equations. These depend on ϕ_i, k_i and on the geometry of Ω^ε. We follow closely [11].

First we formalize the notion of periodicity and heterogeneity in Ω. Without loss of generality we assume that Ω_1^ε is globally connected and $\phi_3 = 0$; all other coefficients in (3.1) are positive constants. We follow the usual structure [1, 11, 12]. Let the unit cube $Y = (0,1)^d \subset \mathbb{R}^d$ be divided into three distinct regions Y_1, Y_2, and Y_3, such that $\partial Y_1 \cap \partial Y_2 = \emptyset$ and $\overline{Y} = \cup_{i=1}^3 \overline{Y}_i$ as illustrated by Figure 1(b). Denote by C_i the characteristic function of Y_i, $i = 1, 2, 3$, extended Y-periodically to all $\mathbb{R}^d$. We assume that the domains $\{x \in \mathbb{R}^d : C_i(x) = 1\}$,

$i = 1,2,3$, have a smooth boundary. Also, we define the ε-periodic characteristic functions $C_i^\varepsilon(x) = C_i(x/\varepsilon)$, $i = 1,2,3$, $x \in \Omega$. Thus, for a fixed ε, Ω is subdivided into three distinct regions $\Omega_i^\varepsilon = \{x \in \Omega : C_i^\varepsilon(x) = 1\}$, $i = 1,2,3$. Another subdivision of Ω is into $O(\varepsilon^{-d})$-periodic cells.

Macroporosities $\widetilde{\phi}_i$

From [11, *equation 16*, page 206] we have $\widetilde{\phi}_i = \int_{Y_i} \phi_i(y)dy$.

Macroconductivities $\widetilde{k}_i$

From [11, *equations 16, 14*, page 205-206] we have

$$\widetilde{k}_p(i,j) = \int_{Y_p} k_p(y)\left(\vec{e}_i + \nabla W_i^p(y)\right)\cdot\left(\vec{e}_j + \nabla W_j^p(y)\right)dy, \quad p = 1,2;\ i,j = 1,\dots d, \tag{3.2}$$

where W_i^p, for $p = 1,2;\ i = 1,\dots,d$, is the solution to an auxiliary PDE

$$\nabla\cdot\left[k_p\left(\vec{e}_i + \nabla W_i^p(y)\right)\right] = 0, \quad \text{in } Y_p, \tag{3.3a}$$

$$k_p\left(\vec{e}_i + \nabla W_i^p(y)\right)\cdot\vec{n}_p = 0, \quad \text{on } \Gamma_{p,3}, \tag{3.3b}$$

$$W_i^p,\ k_p\nabla W_i^p\cdot\vec{n}_p \text{ are periodic.} \tag{3.3c}$$

One can prove [1, 3, 11] that $\widetilde{k}_p$ is a symmetric matrix.

Now consider $d = 2$. Here the region Ω_2^ε cannot be connected. Thus, the boundary condition (3.3c) does not apply and (3.3a), (3.3b), and (3.3c) admit the trivial solution $\vec{e}_i + \nabla W_i^2(y) \equiv 0$ for $i = 1,2$. Consequently, $\widetilde{k}_2$ is the 2×2 null matrix, and the model (1.2a) and (1.2b) becomes the Warren-Root model (3) proposed in [6].

Exchange Term Parameter c

In general, the flow between Ω_1 and Ω_2 *across* Ω_3 has transient character, and an appropriate term describing it must be nonlocal in nature.

However, for very small ϕ_3, the flow is of quasistatic nature as discussed in [4]. The exchange term then has the form $c(\widetilde{\rho}_1 - \widetilde{\rho}_2)$. To compute c, we consider the solution U of

$$-\nabla\cdot[k_3\nabla U] = 0, \quad \text{in } Y_3, \tag{3.4a}$$

$$U = 1, \quad \text{on } \Gamma_{1,3}, \tag{3.4b}$$

$$U = 0, \quad \text{on } \Gamma_{2,3}, \tag{3.4c}$$

$$U,\ k_3\nabla U\cdot\vec{n}_3 \text{ are periodic on } \Gamma_{3,3}. \tag{3.4d}$$

The parameter c see [11, *equation 19*, page 209] is given by

$$c = \int_{\Gamma_{1,3}} k_3 \nabla_y U \cdot \vec{n}_3 ds. \tag{3.5}$$

We note that the general non-quasistatic case is when $\phi_3(\partial U/\partial t)$ is included in (3.4d) thereby changing the character of exchange term to nonlocal. Conversely, (3.4a), (3.4b), (3.4c), and (3.4d) can be considered as its special case when $\phi_3 \approx 0$.

3.1.2. Numerical Computation of Macro-Model Parameters

The solutions of the auxiliary PDEs (3.3a), (3.3b), and (3.3c) and (3.4a), (3.4b), (3.4c), and (3.4d) are approximated using finite elements with $h_{k_1}^{-1} = 40$ and $h_c^{-1} = 20$. See [36] for treatment of periodic boundary conditions.

In what follows we ignore the distinction between the exact and numerical values of macro-model parameters $\widetilde{k}_i$, c and provide examples of their calculations for various values of k_3 and choices of geometry of Y.

In all examples $d = 2$ hence $\widetilde{k}_2 = \left[\begin{smallmatrix} 0 & 0 \\ 0 & 0 \end{smallmatrix}\right]$. Also, in all examples $k_1 \equiv$ const and the geometry of Y is axisymmetric, and thus $\widetilde{k}_1$ is a scalar constant.

Example 3.1. Here $Y_2 = (0.3, 0.7)^2$, $Y_3 = (0.2, 0.8)^2 \setminus Y_2$, $\phi = 1\chi_1 + 10^{-4}\chi_2$, and $k = 1\chi_1 + 10^{-4}\chi_2 + 10^{-7}\chi_3$. We obtain

$$\widetilde{\phi}_1 = 0.64, \qquad \widetilde{\phi}_2 = 1.6 \times 10^{-5}, \qquad \widetilde{k}_1 = 0.4519, \qquad c = 1.8634 \times 10^{-6}. \tag{3.6}$$

Example 3.2. Let $Y_2 = (0.3, 0.7)^2$, $Y_3 = (0.2, 0.8)^2 \setminus Y_2$. $\phi = 1\chi_1 + 10^{-4}\chi_2$, and $k = 1\chi_1 + 10^{-1}\chi_2 + 10^{-4}\chi_3$. We obtain

$$\widetilde{\phi}_1 = 0.64, \qquad \widetilde{\phi}_2 = 1.6 \times 10^{-5}, \qquad \widetilde{k}_1 = 0.4519, \qquad c = 1.8634 \times 10^{-3}. \tag{3.7}$$

Example 3.3. Here $Y_2 = (0.3, 0.7)^2$, $Y_3 = (0.2, 0.8)^2 \setminus Y_2$, $\phi = 1\chi_1 + 10^{-4}\chi_2$, and $k = 1\chi_1 + 10^{-1}\chi_2 + 10^{-2}\chi_3$. We obtain

$$\widetilde{\phi}_1 = 0.64, \qquad \widetilde{\phi}_2 = 1.6 \times 10^{-5}, \qquad \widetilde{k}_1 = 0.4519, \qquad c = 1.8634 \times 10^{-1}. \tag{3.8}$$

Example 3.4. Let $Y_2 = (0.3, 0.7)^2$, $Y_3 = (0.1, 0.9)^2 \setminus Y_2$, $\phi = 1\chi_1 + 10^{-4}\chi_2$, and $k = 1\chi_1 + 10^{-1}\chi_2 + 10^{-4}\chi_3$. We get

$$\widetilde{\phi}_1 = 0.36, \qquad \widetilde{\phi}_2 = 1.6 \times 10^{-5}, \qquad \widetilde{k}_1 = 0.2130, \qquad c = 1.0412 \times 10^{-3}. \tag{3.9}$$

Example 3.5. $Y_2 = (0.25, 0.75)^2$, $Y_3 = (0.2, 0.8)^2 \setminus Y_2$, $\phi = 1\chi_1 + 10^{-4}\chi_2$, and $k = 1\chi_1 + 10^{-1}\chi_2 + 10^{-4}\chi_3$. We get

$$\widetilde{\phi}_1 = 0.64, \qquad \widetilde{\phi}_2 = 2.5 \times 10^{-5}, \qquad \widetilde{k}_1 = 0.4519, \qquad c = 4.3000 \times 10^{-3}. \tag{3.10}$$

3.2. Comparison of the Models

Now we can compare the solutions of the micro-model (1.1) to those of the macro-model (1.2a) and (1.2b). In [11] it was shown that the latter two-scale converge to the former as $\varepsilon \to 0$. In addition, the analysis in [11] suggests that it is appropriate to compare $\widetilde{\rho}_i$ to $\chi_i \rho_\varepsilon$. However, this notion of convergence does not give information about the rate at which $\widetilde{\rho}_i - \chi_i \rho_\varepsilon$ may converge, and it involves special periodic test functions.

In this paper we estimate this rate by comparing their numerical approximations directly without the use of any test functions but rather in a certain metric of interest. To the best of our knowledge such comparison or convergence rate was not discussed elsewhere.

Strictly speaking, the two-scale convergence proof considered in [11], and a similar proof for the double-porosity model in [12], includes scaling of k_3 with ε^2. This scaling is a formal device necessary to preserve certain parts of the boundary value problem under investigation in the limit as $\varepsilon \to 0$. However, the homogenization limit is intended to serve only as an *approximation* of the true model, which has a given fixed set of parameters. We do not include this scaling in our computations. Rather, we treat each example, for a given ε, as a data set in its own merit, rather than as an element of a sequence intended to two-scale converge to the limit.

3.2.1. Setup of Computational Experiments

We set up simulations for comparison using compatible data for micro- and macro-models; we set $f \equiv 0$ and choose initial and boundary data driving the flow with interesting dynamics. For porosities and conductivities, we use the values computed in Section 3.1.2.

Let $\Omega = (0,1)^2$ and $\Gamma_D = \{0\} \times [0,1] \cup \{1\} \times [0,1]$. On Γ_D we define $\rho_D(0,y) = 1$, $\rho_D(1,y) = 0$, $y \in [0,1]$. On the lateral sides of Ω the Neumann no-flow condition is imposed. Also, let $\rho_0 \equiv 1$. Thus the flow in the micro-model goes from left to right, and the solution evolves towards the stationary solution $\langle 1-x, 1-x \rangle$. Due to the incompatibility between initial and boundary data, we have high gradients of the solution close to $x = 1$ for small t.

We fix the final time $T = 0.05$ and use uniform time stepping with $\Delta t = 10^{-4}$. The solution of the micro-model ρ depends on the number of cells in $\Omega \equiv \Omega^\varepsilon$, with $\varepsilon \in (0,1]$. For example, if $\varepsilon = 1/2$, the domain Ω is composed of $2 \times 2 = 4$ cells. We denote the numerical solution of (2.8a) and (2.8b) at t_n by $\rho^n_{\varepsilon,h}$ where h denotes the grid parameter for the micro-model.

For the macro-model, we use $\widetilde{\rho}_{i,0} = \rho_0 \equiv 1$. Also, we use $\widetilde{\rho}_{D,i} = \rho_D$ for $i = 1,2$ when $\widetilde{k}_2 \not\equiv 0$. If $\widetilde{k}_2 \equiv 0$, then the boundary condition for $\widetilde{\rho}_2$ is not prescribed.

3.2.2. Qualitative Comparison

In our first comparison we use parameters from Example 3.1. We solve the macro-model (4.2) for $\{\langle \widetilde{\rho}^n_{1,h_1}, \widetilde{\rho}^n_{2,h_2} \rangle\}_{n=1}^N$ and the micro-model (2.8a) and (2.8b) for $\rho^n_{\varepsilon,h}$. The plots of ρ^n_h and $\widetilde{\rho}^n_{i,h}$ are in Figure 2, and a different view is shown in Figure 1(d).

The heterogeneous structure of Ω^ε is well visible from the behavior of the micro-model solution ρ^n_h. Large gradients of solution are visible on cell boundaries due to the large difference between k_1, k_2, and k_3.

However, the behavior in the fast region is well approximated by $\widetilde{\rho}^n_{1,h_1}$ which envelopes $\rho^n_h \chi_1$, while $\widetilde{\rho}^n_{2,h_2}$ envelopes $\rho^n_h \chi_2$ well. This is very well seen in a side view in Figure 2(d).

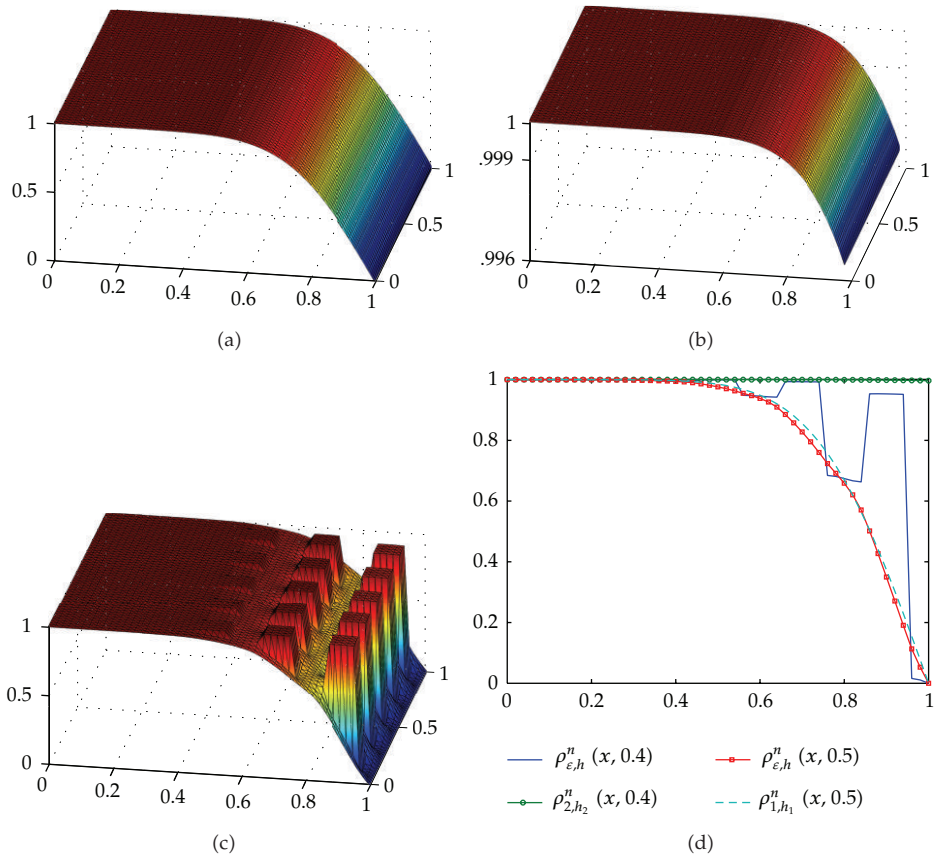

Figure 2: Numerical approximation at $t_n = 3 \times 10^{-2}$ of (a)-(b) the solutions of the two components of the macro-model (4.2), and (c) the solutions of the micro-model (2.8a) and (2.8b). Figure (d) shows the side view of (a, b, c) at $y = 0.4$ and $y = 0.5$. Data from Example 3.1 with $1/\varepsilon = 5$ and $h = h_1 = h_2 = 1/50$. Note that (a) and (b) have different vertical scales.

Quite interesting is the behavior of $\rho_2|_{x=1}$. Since in our examples $\tilde{k}_2 \equiv 0$, no boundary condition at $x = 1$ is imposed on ρ_2. Thus, for small t, $\rho_2(1, t)$ evolves from its initial constant value of 1 according to (1.3b) with the input from $\tilde{\rho}_1$. The latter satisfies, however, the homogeneous boundary condition at $x = 1$. In particular, with constant $\tilde{\phi}_2$, c, we have

$$\tilde{\rho}_2(x, y, t) = \tilde{\rho}_{2,0}(x, y) e^{-(c/\tilde{\phi}_2)t} + \int_0^t \tilde{\rho}_1(x, y, s) e^{-(c/\tilde{\phi}_2)(t-s)} ds. \tag{3.11}$$

Thus, for small t and small $c/\tilde{\phi}_2$, $\tilde{\rho}_2(1, y, t)$ is away from 0, but, as time increases, its magnitude decreases proportionally to $e^{-(c/\tilde{\phi}_2)t}$.

Next, we use parameters from Example 3.2 and plot them in Figure 3. In this example the conductivity k_1 is much larger than that of previous case, the local gradients in the micro-model are smaller, and the solutions to the macro-model achieve a smoother profile faster.

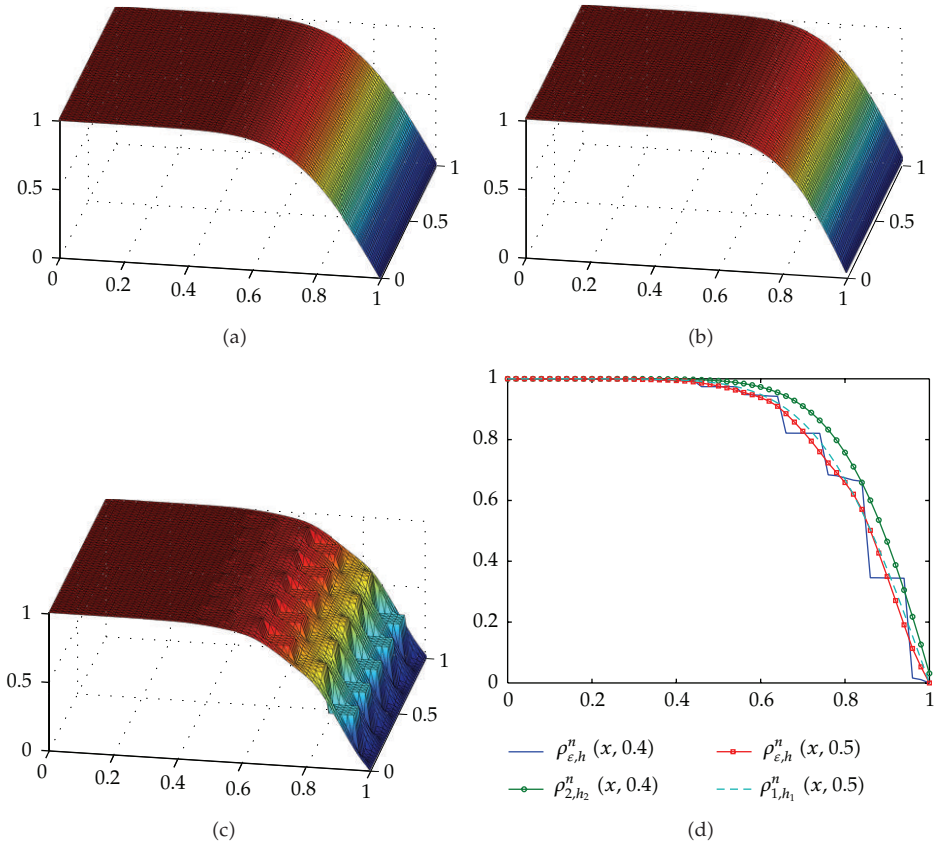

Figure 3: Numerical approximation at $t_n = 3 \times 10^{-2}$ of (a) and (b) the solutions of the two components of the macro-model (4.2) and (c) the solutions of the micro-model (2.8a) and (2.8b). Figure (d) shows the side view of (a, b, c) at $y = 0.4$ and $y = 0.5$. Data from Example 3.2 with $1/\varepsilon = 5$ and $h = h_1 = h_2 = 1/50$.

3.2.3. Quantitative Comparison—Fine Grid in Macro-Model

Now we are ready to discuss a quantitative comparison between solutions to the micro- and macro-models. For this, we set up a family of cases with $\varepsilon = 1/(2l+1)$, $l \geq 1$. We use uniform mesh with $h = h_1 = h_2 = \varepsilon/20$ for now. See Section 3.2.4 for $h_i \gg h$ and Section 4 for adaptive gridding.

From [11, Theorem 18, page 208] and from our plots it follows that we can actually compare the micro- and macrosolutions, as long as the characteristic functions χ_i are involved. While the results in [11] use two-scale convergence with ε, that is, rely on special periodic test functions, we compare $\rho^n_{\varepsilon,h}$ and $\tilde{\rho}^n_{i,h}$ directly. We see that it is easy to do so only in the connected region Ω_1.

We define a quantity $e^n_\varepsilon = (\rho^n_{\varepsilon,h} - \tilde{\rho}^n_{1,h_1})\chi_1$ to be used in comparison. We also define, for a fixed $t \in (0, T]$ and some function z,

$$\|z(x,y;t)\|_{*,L_1} := \int_0^1 |z(x,0.5;t)|dx,$$

Table 1: Comparison of solutions to the macro-model with those to the micro-model for different values of ε with data as in Example 3.2.

# cells	ε	$\|e_\varepsilon^N\|_{*,L_1}$	α_1	$\|e_\varepsilon^N\|_{*,L_2}$	α_2
3×3	$1/3$	1.1832×10^{-2}	—	3.2071×10^{-2}	—
5×5	$1/5$	7.0915×10^{-3}	1.0188	1.9044×10^{-2}	1.0390
7×7	$1/7$	5.0522×10^{-3}	1.0077	1.3528×10^{-2}	1.0164
9×9	$1/9$	3.9285×10^{-3}	1.0011	1.0502×10^{-2}	1.0075
11×11	$1/11$	3.2162×10^{-3}	0.9969	8.5890×10^{-3}	1.0021

Table 2: Comparison of the macro-model to the micro-model for different values of ε as in Example 3.3.

# cells	ε	$\|e_\varepsilon^N\|_{*,L_1}$	α_1	$\|e_\varepsilon^N\|_{*,L_2}$	α_2
3×3	$1/3$	1.1446×10^{-2}	—	3.0715×10^{-2}	—
5×5	$1/5$	7.0065×10^{-3}	1.0408	1.8387×10^{-2}	0.9956
7×7	$1/7$	5.1541×10^{-3}	1.0958	1.3363×10^{-2}	1.0543
9×9	$1/9$	4.1704×10^{-3}	1.1867	1.0684×10^{-2}	1.1232
11×11	$1/11$	3.5794×10^{-3}	1.3131	9.0460×10^{-3}	1.2058

$$\left\|z(x,y;t)\right\|_{*,L_2} := \left\{\int_0^1 |z(x,0.5;t)|^2 dx\right\}^{1/2}, \tag{3.12}$$

which will be applied to e_ε^n. Clearly $\|\cdot\|_{*,W}$ is not a norm but is a useful quantity of interest.

In Tables 1, 2, 3, and 4 we present $\|e_\varepsilon^n\|_{*,W}$ for different ε and $W = L_2, L_1$. For each case we consider convergence of $\|e_\varepsilon^n\|_{*,W}$ with $\varepsilon \downarrow 0$.

From homogenization theory it is not clear what order of convergence should be expected. We observe that $\|e_\varepsilon^n\|_{*,W}$ decreases linearly with ε for both $* = L_1, L_2$ -like quantities in all cases.

Next we discuss the dependence of the results on conductivity and other data. Consider Example 3.2 as a reference example with its corresponding Table 1. Compare it now with that from Table 2 where k_3 is larger than that in the reference case to see how this influences the errors. As expected, and as shown in Example 3.3, c changes by the same factor, and this means that the coupling between $\tilde{\rho}_1$ and $\tilde{\rho}_2$ is stronger which corresponds to faster flow across Y_3 in the micro-model. However, the influence on the convergence of the micro-macro difference, from Table 2 is rather weak.

Next consider Example 3.4 which uses a different geometry than that in the reference case, with thicker region Y_3. This produces a slightly smaller c since the gradient of U is smaller. Also, $\tilde{\phi}_1$ and $\tilde{k}_1$ are predictably different. The error quantity is influenced insignificantly.

The opposite effect is seen in Table 4 when Y_3 is selected as thinner than in the reference Example 3.2.

3.2.4. Coarse Macrogrid and Parameter Grid

In the examples presented in Section 3.2.3 we used $h = h_1 = h_2$. This choice of compatible grids is convenient for visualization purposes. However, for the idea of the macro-model to

Table 3: Comparison of the macro-model to the micro-model for different values of ε Example 3.4.

# cells	ε	$\|e_\varepsilon^N\|_{*,L_1}$	α_1	$\|e_\varepsilon^N\|_{*,L_2}$	α_2
3×3	$1/3$	1.3758×10^{-2}	—	3.5390×10^{-2}	—
5×5	$1/5$	8.2810×10^{-3}	1.0330	2.0998×10^{-2}	0.9786
7×7	$1/7$	5.7341×10^{-3}	0.9155	1.4741×10^{-2}	0.9510
9×9	$1/9$	4.3987×10^{-3}	0.9479	1.1336×10^{-2}	0.9568

Table 4: Comparison of the macro-model to the micro-model for different values of ε Example 3.5.

# cells	ε	$\|e_\varepsilon^N\|_{*,L_1}$	α_1	$\|e_\varepsilon^N\|_{*,L_2}$	α_2
3×3	$1/3$	1.1826×10^{-2}	—	3.2048×10^{-2}	—
5×5	$1/5$	7.0877×10^{-3}	0.9978	1.9029×10^{-2}	0.9800
7×7	$1/7$	5.0497×10^{-3}	0.9924	1.3518×10^{-2}	0.9840
9×9	$1/9$	3.9281×10^{-3}	1.0006	1.0502×10^{-2}	0.9955

be useful, the computational complexity of the macro-model needs to be lower than that of the micro-model. Since the macro-model is a system of two equations, its lower complexity can be only achieved if the grid in the macro-model is significantly coarser than that of micro-model. Below we show that one can use $h \ll h_1$ in the macro-model.

Example 3.6. We use data from Example 3.2 with $\varepsilon = 0.2$. Consider a fixed microgrid with $h^{-1} = 100$ and a few cases of macrogrid with $h_1^{-1} = h_2^{-1} = 10, 50, 100$. Now we compare the micro- and macrosolutions $\rho^n_{\varepsilon,h}$ and ρ_{1,h_1}, see Table 5. We also compare the run time of the macro-model to that of the reference micro-model which is 120 seconds.

We see that, as predicted above, the macro-model run time at $h_i = h$ is not competitive with that of the micro-model; this is exacerbated by the overhead of various adaptive procedures to be discussed below. However, when $h_i \gg h$, the ability of the macro-model solutions to approximate those of micro-model appears reasonable and is associated with a much lower cost. This is true even when h_i is by a factor of 10 coarser than h resulting in a computational time decreased by two orders of magnitude.

Clearly, the macro-model can run much faster than the micro-model especially when adaptive nonuniform grids with $h_1 \neq h_2$ are implemented, see Section 4.

Influence of Parameter Grid

Last we address the effect of the computed parameters c, $\widetilde{k}_1$ on the closeness of the macro-model solution to that of micro-model. These coefficients are precomputed as discussed in Section 3.1.1.

Example 3.7. Let $\varepsilon = 1/3$, and let the micro-model grid be $h^{-1} = 60$. Use $h_1^{-1} = h_2^{-1} = 60$. Compute numerical parameters c_{h_c}, $\widetilde{k}_{1,h_{k_1}}$ by approximating solutions to (3.4a), (3.4b), (3.4c), and (3.4d) and (3.3a), (3.3b), and (3.3c), respectively.

Example 3.7 and Table 6 show that the grid used for computing these parameters only mildly affects the quality of the solution, thus one can use coarse grid with confidence.

Table 5: Comparison of the micro-model to the macro-model as in Example 3.6.

h_1^{-1}	$\|e_\varepsilon^N\|_{*,L_1}$	$\|e_\varepsilon^N\|_{*,L_2}$	run time(s)
100	7.0915×10^{-3}	1.9044×10^{-2}	511
50	7.0937×10^{-3}	1.9048×10^{-2}	56
10	7.2380×10^{-3}	1.9173×10^{-2}	3

Table 6: Sensitivity of the macro-model solution to the grid used to compute $c_{h_c} \approx c$ and $\widetilde{k}_{1,h_{k_1}} \approx \widetilde{k}_1$ as Example 3.7.

h_c^{-1}	c_{h_c}	$\|e_\varepsilon^N\|_{*,L_1}$	$\|e_\varepsilon^N\|_{*,L_2}$
10	1.9000×10^{-3}	3.6251×10^{-2}	5.9026×10^{-2}
50	1.8370×10^{-3}	3.6251×10^{-2}	5.9026×10^{-2}
100	1.8292×10^{-3}	3.6251×10^{-2}	5.9026×10^{-2}
200	1.8258×10^{-3}	3.6251×10^{-2}	5.9026×10^{-2}
h_k^{-1}	$\widetilde{k}_1(1,1)$	$\|e_\varepsilon^N\|_{*,L_1}$	$\|e_\varepsilon^N\|_{*,L_2}$
10	4.6306×10^{-1}	3.5392×10^{-2}	5.7835×10^{-2}
50	4.5141×10^{-1}	3.6222×10^{-2}	5.8989×10^{-2}
100	4.5046×10^{-1}	3.6301×10^{-2}	5.9093×10^{-2}
200	4.5009×10^{-1}	3.6332×10^{-2}	5.9134×10^{-2}

4. Error Estimates and Two-Grid Adaptivity

We present now the details of discrete formulation of (2.4) using independent grids for each component and adaptive gridding. The adaptive two-grid algorithm further reduces the computational cost of the macro-model. The formalism of the two-grid solution connects loosely to [37, 38] where their benefit was considered for a nonlinear scalar equation.

In what follows we assume that $\widetilde{k}_1 \gg \widetilde{k}_2$, that is, that the first component varies in space faster than the second. As a special case, this includes the case $\widetilde{k}_2 = 0$. We consider two triangulations $\mathcal{T}_{h_i}$, $i = 1, 2$, which will be used for $\widetilde{\rho}_{h_i}$, respectively. In principle, these can be chosen independently. In fact, we allow the triangulations to vary in time and thus consider $\mathcal{T}_{h_i}^n$ and the associated spaces $V_{h_i}^n$ as in (2.7). To avoid the loss of accuracy due to excessive interpolation and intergrid projections and because $\widetilde{k}_1 \gg \widetilde{k}_2$, we assume that $\mathcal{T}_{h_1}^n$ is a refinement of the partition $\mathcal{T}_{h_2}^n$.

We need intergrid operators to handle two components that live on separate grids. Let $\Pi : V_{h_2}^n \to V_{h_1}^n$ be the interpolation operator and $\Pi' : V_{h_1}^n \to V_{h_2}^n$ the L_2 projection defined by

$$\left(\Pi'_{\phi_{h_1},\psi_{h_2}}\right) := (\phi_{h_1}, \Pi_{\psi h_2}), \quad \forall \psi_{h_2} \in V_{h_2}. \tag{4.1}$$

Now we define the discrete solutions. At each time step $1 \le n \le N$, we seek $\widetilde{\rho}_{i,h_i}^n \in V_{h_i}^n$, $i = 1, 2$, which satisfy the discrete problem, that is, (2.4) restricted to the finite dimensional subspaces $V_{h_i}^n$ so that, for all $\psi_{h_1} \in V_{h_1}^n$, for all $\xi_{h_2} \in V_{h_2}^n$

$$\left(\widetilde{\phi}_1 \frac{\widetilde{\rho}_{1,h_1}^n - \widetilde{\rho}_{1,h_1}^{n-1}}{\Delta t_n}, \psi_{h_1}\right) + \left(\widetilde{k}_1 \nabla \widetilde{\rho}_{1,h_1}^n, \nabla \psi_{h_1}\right) + \left(c\left(\widetilde{\rho}_{1,h_1}^n - \Pi \widetilde{\rho}_{2,h_2}^n\right), \psi_{h_1}\right) = (f, \psi_{h_1}),$$

$$\left(\widetilde{\phi}_2 \frac{\widetilde{\rho}^n_{2,h_2} - \widetilde{\rho}^{n-1}_{2,h_2}}{\Delta t_n}, \xi_{h_2}\right) + \left(\widetilde{k}_2 \nabla \widetilde{\rho}^n_{2,h_2}, \nabla \xi_{h_2}\right) + \left(c\left(\widetilde{\rho}^n_{2,h_2} - \Pi' \widetilde{\rho}^n_{1,h_1}\right), \xi_{h_2}\right) = 0,$$

$$\left\langle \widetilde{\rho}^0_{1,h_1}, \widetilde{\rho}^0_{2,h_2} \right\rangle = \left\langle \mathcal{I}_{h_1} \widetilde{\rho}_{1,0}, \mathcal{I}_{h_2} \widetilde{\rho}_{2,0} \right\rangle \quad \text{in } \Omega. \tag{4.2}$$

If $\widetilde{k}_2 = 0$, the system (4.2) is modified appropriately so that $\widetilde{\rho}_2(\cdot, t) \in L^2(\Omega)$ instead of $H^1_D(\Omega)$, and we do not impose boundary conditions on this component. In fact, instead of (2.7) we define

$$V^n_{h_2} = \left\{ v_h \in C\left(\overline{\Omega}\right) : \forall T \in \mathcal{T}^n_h,\ v_h\,|_T \in \mathcal{P}_k(T) \right\}. \tag{4.3}$$

(It holds that $v_h \in C(\overline{\Omega})$ but it is not necessary). It is straightforward that (4.2) is uniquely solvable.

4.1. A Priori Error Estimate

We have the following convergence result proved for the error in energy norm. In what follows $1 \le n \le N$ and $i = 1, 2$. We denote $e_{i,h_i}(t_n) = \widetilde{\rho}^n_{i,h_i} - \widetilde{\rho}^n_i$ and define the energy norm for the product space

$$|||\langle z, w \rangle|||^2(t_n) := \widetilde{\phi}_1 \|z(t_n)\|^2 + \widetilde{\phi}_2 \|w(t_n)\|^2 + \sum_{m=1}^{n} \Delta t_m \left(\widetilde{k}_1 |z(t_m)|^2_1 + \widetilde{k}_2 |w(t_m)|^2_1 \right). \tag{4.4}$$

Assuming that $\langle \widetilde{\rho}_1, \widetilde{\rho}_2 \rangle$ is sufficiently smooth we have the following *a-priori* estimate proven in the appendix.

Theorem 4.1. *Let* $\langle \widetilde{\rho}_1, \widetilde{\rho}_2 \rangle$, $\{ \langle \widetilde{\rho}^n_{1,h_1}, \widetilde{\rho}^n_{2,h_2} \rangle \}_{n=1}^N$ *be the smooth solutions of* (2.4) *and* (4.2), *respectively. Then one has*

$$|||\langle e_{1,h_1}, e_{2,h_2} \rangle|||(t_n) \le \widetilde{k}_1^{1/2} C_1 h_1 + \widetilde{k}_2^{1/2} C_2 h_2 + C_3 \max_{m=1:n} \Delta t_m + \textit{higher order terms (h.o.t.)}, \tag{4.5}$$

where C_1, C_2, *and* C_3 *are independent of* h.

Furthermore, if $\widetilde{k}_2 = 0$, *then*

$$|||\langle e_{1,h_1}, e_{2,h_2} \rangle|||(t_n) \le \widetilde{k}_1^{1/2} C_1 h_1 + C_2 h_2^2 + C_3 \max_{m=1:n} \Delta t_m + \textit{higher order terms (h.o.t.)}. \tag{4.6}$$

Now we notice that (4.5) suggests the following choice of grid parameters h_1, h_2. If $\widetilde{k}_1 \gg \widetilde{k}_2$, then to balance the components of the error one can use $h_1 \ll h_2$. Similarly, if $\widetilde{k}_2 = 0$, then (4.6) implies that h_2 can be chosen to be of the order of $h_1^{1/2}$. The use of coarse grid $h_2 \gg h_1$ for the second component reduces the size of the linear system to be solved and decreases the computational time of the macro-model.

Also, the a-priori estimates (4.5), (4.6) are global. One can further reduce the computational cost while maintaining accuracy by using local grid adaptivity guided by a posteriori estimators. This is pursued below.

4.2. A-Posteriori Error Estimates

Estimators for time-dependent problems can be defined in many ways including the now classical space-time element and adjoint approaches [27, 28]. In this paper we follow the residual estimator framework extending [15, 29] to the double-diffusion system using the ideas in [13, 39, 40] originally formulated for an elliptic system.

The estimator $\eta_n = (\sum_{m=1}^{n}[\Delta t_m S_m^2 + T_m^2])^{1/2}$ for (4.2) is composed of the temporal part T_n which adapts the time stepping and the spatial part S_n which guides the spatial grid adaptivity. We define

$$\begin{aligned} T_n^2 := \frac{\Delta t_n}{3}\left(\left\|\tilde{k}_1^{1/2}\left(\tilde{\rho}_{1,h_1}^n - \tilde{\rho}_{1,h_1}^{n-1}\right)\right\|^2 + \left\|\tilde{k}_2^{1/2}\left(\tilde{\rho}_{2,h_2}^n - \tilde{\rho}_{2,h_2}^{n-1}\right)\right\|^2\right) \\ + \frac{\Delta t_n}{3}\left\|c^{1/2}\left(\tilde{\rho}_{1,h_1}^n - \tilde{\rho}_{1,h_1}^{n-1}\right) - c^{1/2}\left(\tilde{\rho}_{2,h_2}^n - \tilde{\rho}_{2,h_2}^{n-1}\right)\right\|^2, \end{aligned} \tag{4.7}$$

and $S_n^2 = S_{1,n} + S_{2,n}$, where $S_{i,n} = \sum_{T_i \in \mathcal{T}_{h_i}} S_{i,T_i}^n$, and where, as usual (see [23]), one defines

$$S_{i,T_i}^n := \theta_{i,T_i}^2 \left\|R_{i,T_i}^n\right\|^2 + \frac{1}{2}\sum_{E \in \mathcal{E}_{T_i}} \gamma_{i,E}^2 \left\|R_{i,E}^n\right\|^2. \tag{4.8}$$

The element and edge residuals in S_{i,T_i}^n, $i = 1, 2$, are given by

$$R_{i,T_i}^n = f_i - \tilde{\phi}_i \frac{\tilde{\rho}_{i,h_i}^n - \tilde{\rho}_{i,h_i}^{n-1}}{\Delta t_n} + \nabla \cdot \left(\tilde{k}_i \nabla \tilde{\rho}_{i,h_i}^n\right) + (-1)^i c\left(\tilde{\rho}_{1,h_1}^n - \tilde{\rho}_{2,h_2}^n\right), \tag{4.9}$$

$$R_{i,E}^n = \begin{cases} \left[\tilde{k}_i \partial_\nu \tilde{\rho}_{i,h_i}^n\right]_E & \text{if } E \not\subset \partial\Omega, \\ -\tilde{k}_i \partial_\nu \tilde{\rho}_{i,h_i}^n & \text{if } E \subset \Gamma_N, \\ 0, & \text{otherwise.} \end{cases} \tag{4.10}$$

Here $[z]_E$ denotes the jump of the flux z across the edge E of an element. Usually $f_1 \equiv f$, $f_2 \equiv 0$. Also, if $\tilde{k}_2 = 0$, then $R_{2,E}^n \equiv 0$.

The scaling constants $\theta_{i,T}$, $\gamma_{i,E}$ take into account the contribution of the exchange term $c(\tilde{\rho}_1 - \tilde{\rho}_2)$ and are defined so that the estimators remain robust when the coefficients of the problem change substantially:

$$\theta_{1,T} = \min\left\{h_{T_1}\tilde{k}_1^{-1/2}, \max\left\{c^{-1/2}, h_{T_1}\tilde{k}_2^{-1/2}\right\}\right\}, \quad T_1 \in \mathcal{T}_{h_1}^n \cup \mathcal{E}_{h_1}^n, \tag{4.11}$$

$$\theta_{2,T} = \min\left\{h_{T_2}\tilde{k}_2^{-1/2}, \max\left\{c^{-1/2}, h_{T_2}\tilde{k}_1^{-1/2}\right\}\right\}, \quad T_2 \in \mathcal{T}_{h_2}^n \cup \mathcal{E}_{h_2}^n, \tag{4.12}$$

$$\gamma_{i,E} = 2h_E^{-1/2}\theta_{i,E}, \quad i = 1, 2. \tag{4.13}$$

This a posteriori estimator works well with two-grid discretizations as shown in the examples to follow. It is well formulated also for $\widetilde{k}_2 \equiv 0$ when $\widetilde{\rho}_2 \in L^2(\Omega)$. We have the following result on reliability of the estimator proven in the appendix.

Theorem 4.2. *Let* $\langle \widetilde{\rho}_1, \widetilde{\rho}_2 \rangle$, $\{\langle \widetilde{\rho}^n_{1,h_1}, \widetilde{\rho}^n_{2,h_2} \rangle\}_{n=1}^N$ *be the solution of* (1.2a) *and* (1.2b), (2.3) *and* (4.2), *respectively. Then*

$$|||\langle e_{1,h_1}, e_{2,h_2} \rangle|||(t_n) \leq \eta_n + h.o.t.; \ \forall n \geq 1 \tag{4.14}$$

4.3. Adaptive Two-Grid Discretization and Implementation

Consider a fixed time step $n = n_o$ for which some triangulation is chosen, the solution is found, and the spatial error indicators $S_{i,n}$ are computed. To apply the two-grid spatial adaptivity we use the following refinement algorithm.

Adaptive Two-Grid Algorithm $\mathcal{A}$

(1) Select the triangulation(s) to be refined: If $S_{1,n_o} > 3S_{2,n_o}$, refine only $\mathcal{T}^{n_o}_{h_1}$. If $S_{2,n_o} > 3S_{1,n_o}$, refine only $\mathcal{T}^{n_o}_{h_2}$. Otherwise, refine both.

(2) In $\mathcal{T}_{h_i}$, $i = 1, 2$ selected in Step 1, refine any $T \in \mathcal{T}_{h,i}$ for which $S^{n_o}_{i,T} \geq 0.5 \max_{T \in \mathcal{T}_{h_i}} S^{n_o}_{i,T}$.

(3) Enforce the requirement that $\mathcal{T}^n_{h_1}$ is a refinement of $\mathcal{T}^n_{h_2}$ by adding extra elements as needed.

The steps in $\mathcal{A}$ should be repeated a certain number $N_{\mathcal{A}}$ of times until an ideal grid is found. See [41] for analysis of whether the iterative process of refinement and coarsening is, in general, convergent.

Example of Two-Grid Adaptivity

Now we show an example on how this adaptive algorithm works for the double-diffusion system. We use data and setup from Example 3.2, with $T = 0.02$ and uniform time stepping with $\Delta t = 10^{-4}$. Other data is as in Section 3.2.1.

Consider a fixed $n_0 = 200$ with a uniform triangulation $\mathcal{T}^{n_o}_{h_1} = \mathcal{T}^{n_o}_{h_2}$ with $h_1 = h_2 = 0.1$. Then apply $N_A = 6$ times the steps in $\mathcal{A}$, see the solution and the refined meshes in Figure 4. The process works as expected: since at the time t_{n_0} the solution has a high gradient near $x = 1$, the refinement occurs there. The refinement affects the grid for the first component only, because the gradients of the second component are not included due to $\widetilde{k}_2 = 0$. This can be compared to the *a-priori* estimate in Theorem 4.1 from which we know the convergence is $O(h_1 + h_2^2 + \Delta t_n)$.

In Table 7 we provide the details on $\mathcal{T}^{n_o}_{h_i}$ and compare the effectiveness of the local two-grid refinement by algorithm $\mathcal{A}$ with uniform grid refinement. With adaptive refinement we get $S_{n_o} = 0.35834$ with $435 + 121 = 556$ unknowns, while the uniform refinement needs $441 + 441 = 882$ unknowns to achieve comparable $S_{n_o} = 0.39221$.

Last, we describe the process with which $\mathcal{T}^n_{h_i}$, $i = 1, 2$, may vary between time steps. For a fixed n denote by $\mathcal{T}^n_{h_i}$ the final triangulation obtained by the adaptive algorithm $\mathcal{A}$. For the new time step $n + 1$, we use $\mathcal{T}^n_{h_i}$ as the initial triangulation. If the algorithm $\mathcal{A}$ suggests that $\mathcal{T}^{n+1}_{h_i}$ is modified, we need to project $\widetilde{\rho}^n_{i,h_i}$ to the new grid so it can be used as initial

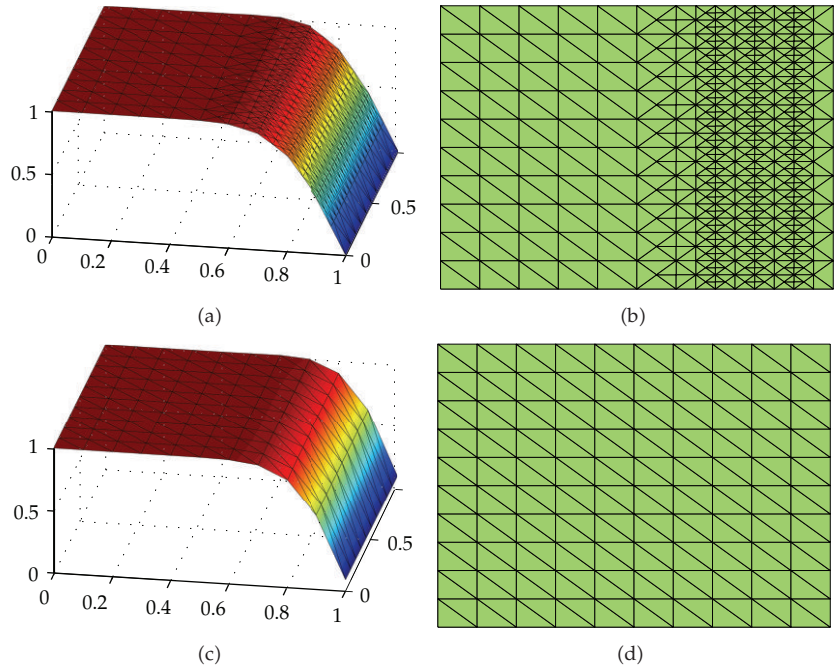

Figure 4: Sixth level refinement iteration at $t_{n_o} = 2 \times 10^{-2}$. Figures (a) and (b): plots of $\tilde{\rho}^{n_o}_{1,h_1}$ and $\mathcal{T}^{n_o}_{h_1}$. Figures (c), (e), and (d): plots of $\tilde{\rho}^{n_o}_{2,h_2}$ and $\mathcal{T}^{n_o}_{h_2}$.

Table 7: Adaptive versus uniform refinement.

		Uniform refinement			
	S_{n_o}	# elem $\mathcal{T}^{n_o}_{h_1}$	# elem $\mathcal{T}^{n_o}_{h_1}$	$\dim(V^{n_o}_{h_1})$	$\dim(V^{n_o}_{h_2})$
Initial mesh	0.81803	200	200	121	121
1st refinement	0.39221	800	800	441	441
		Adaptive refinement			
	S_{n_o}	# elem $\mathcal{T}^{n_o}_{h_1}$	# elem $\mathcal{T}^{n_o}_{h_2}$	$\dim(V^{n_o}_{h_1})$	$\dim(V^{n_o}_{h_1})$
Initial mesh	0.8180	200	200	121	121
1st level	0.8031	240	200	141	121
2nd level	0.7076	292	200	167	121
3rd level	0.6499	316	200	179	121
4th level	0.5525	462	200	254	121
5th level	0.4205	720	200	385	121
6th level	0.3583	820	200	435	121

data for the new step, but $\tilde{\rho}^{n}_{i,h_i}$ differs from their interpolation only in the elements where the triangulation is coarsened. Another way to deal with different triangulations $\mathcal{T}^{n+1}_{h_i}$, $\mathcal{T}^{n}_{h_i}$ is to compute the a posteriori error estimator in a common refinement of the two triangulations $\mathcal{T}^{n+1}_{h_i}$, $\mathcal{T}^{n}_{h_i}$ [29, 42], but this will not be pursued further.

Table 8: Cost of one-grid versus two-grid discretization in a simulation with 1,000 time steps.

One-grid with $h_1 = h_2 = 1/80$	
Matrix	Cost (seconds)
$S_{1,h_1} + M_{1,h_1}$	3.6547
$B_{\text{one-grid}}$	0.0123
Solve $\mathbb{S}_{\text{one-grid}}$ 1,000 times	0.2761 × 1,000
Total	279.7670
Two-grid with $h_1 = 1/80, h_2 = 1/20$	
Matrix	Cost (seconds)
$S_{1,h_1} + M_{1,h_1}$	3.6547
M_{2,h_2}	0.0438
$\mathbb{I}_{h_1,h_2}$	0.2121
$B_{\text{two-grid}}$	0.0063
Solve $\mathbb{S}_{\text{two-grid}}$ 1,000 times	0.1030 × 1,000
Total	106.9169

Implementation

The decision to use two grids implies that we have to interpolate between the finite element spaces $V_{h_1}^n$ and $V_{h_2}^n$, see (4.1). Suppose that $\{\zeta_{i,j}\}_j$, $i = 1, 2$, is a basis for $V_{h_i}^n$. Then the operator Π in (4.1) is represented by the matrix $\mathbb{I}_{h_1,h_2}$ whose components are given by $\mathbb{I}_{h_1,h_2}(j,k) = (\zeta_{1,j}, \zeta_{2,k})$.

Consider now and compare the computational cost associated with one-grid and two-grid approaches. To solve (4.2) with one-grid $V_{h_1}^n$ we need to assemble the stiffness matrix $S_{1,h_1}(j,k) = (\tilde{k}_1 \nabla\zeta_{1,j}, \nabla\zeta_{1,k})$, the mass matrix $M_{1,h_1}(j,k) = (\zeta_{1,j}, \zeta_{1,k})$, and the block matrix

$$B_{\text{one-grid}} = \begin{bmatrix} -\Delta t S_{1,h_1} + \left(\tilde{\phi}_1 + c\Delta t\right) M_{1,h_1} & -c\Delta t M_{1,h_1} \\ -c\Delta t M_{1,h_1} & \left(\tilde{\phi}_2 + c\Delta t\right) M_{1,h_1} \end{bmatrix}. \tag{4.15}$$

At each time step we solve the linear system with $B_{\text{one–grid}}$; this is referred to as $\mathbb{S}_{\text{one-grid}}$.

To solve (4.2) with two grids and two spaces $V_{h_1}^n, V_{h_2}^n$, we need to assemble the stiffness matrix $S_{1,h_1}(j,k) = (\tilde{k}_1 \nabla\zeta_{1,j}, \nabla\zeta_{1,k})$, the mass matrices $M_{1,h_1}(j,k) = (\zeta_{1,j}, \zeta_{1,k})$, $M_{2,h_2}(j,k) = (\zeta_{2,j}, \zeta_{2,k})$, the interpolation matrix $\mathbb{I}_{h_1,h_2}(j,k) = (\zeta_{1,j}, \zeta_{2,k})$, and the block matrix

$$B_{\text{two-grid}} = \begin{bmatrix} -\Delta t S_{1,h_1} + \left(\tilde{\phi}_1 + c\Delta t\right) M_{1,h_1} & -c\Delta t \mathbb{I}_{h_1,h_2}^T \\ -c\Delta t \mathbb{I}_{h_1,h_2} & \left(\tilde{\phi}_2 + c\Delta t\right) M_{2,h_2} \end{bmatrix}. \tag{4.16}$$

To finish we solve the linear system which we refer to as $\mathbb{S}_{\text{two-grid}}$.

Suppose now we solve (4.2) and wish to maintain $S_n \leq \delta$ for some tolerance δ over 1,000 time steps. With data as in Section 3.1.2 we run the simulations using one grid and find that we need $h_1 = h_2 = 1/80$. Using the two-grid approach we only need $h_1 = 1/80, h_2 = 1/20$.

The computational time needed to assemble the matrices and solve the systems in our MATLAB implementation is displayed in Table 8. Clearly the assembly process takes more

time for two-grid case than for one-grid discretization. However, the economy in the cost of solving the linear system makes up for that cost.

5. Conclusions

We compared the solutions to the micro-model to those of the macro-model and have shown that the latter is a good approximation to the former. This remains true also when a very coarse computational grid is used. Moreover, we established a linear convergence rate in function of the periodicity parameter ε in a certain quantity of interest which further shows that the double-diffusion model is an excellent approximation to the micro-model, at least for the considered scenarios.

To make the double-diffusion model computationally efficient, we proposed an algorithm for local grid adaptivity which allows each component to live on its own grid. The grid refinement is guided by an a posteriori error estimator for which we proved theoretical results.

Appendix

A. Proof of Theorem 4.1

Proof. The proof follows the techniques presented in [25, 26] for a scalar PDE. We present an outline of the proof for the double-diffusion system. By (4.1), if $\mathcal{T}_{h_1}^n$ is a refinement of $\mathcal{T}_{h_2}^n$, we can rewrite (4.2) as

$$\begin{aligned}\left(\tilde{\phi}_1 \frac{\tilde{\rho}_{1,h_1}^n - \tilde{\rho}_{1,h_1}^{n-1}}{\Delta t_n}, \psi_{h_1}\right) + \left(\tilde{k}_1 \nabla \tilde{\rho}_{1,h_1}^n, \nabla \psi_{h_1}\right) + \left(c\left(\tilde{\rho}_{1,h_1}^n - \tilde{\rho}_{2,h_2}^n\right), \psi_{h_1}\right) &= (f, \psi_{h_1}),\\ \left(\tilde{\phi}_2 \frac{\tilde{\rho}_{2,h_2}^n - \tilde{\rho}_{2,h_2}^{n-1}}{\Delta t_n}, \xi_{h_2}\right) + \left(\tilde{k}_2 \nabla \tilde{\rho}_{2,h_2}^n, \nabla \xi_{h_2}\right) + \left(c\left(\tilde{\rho}_{2,h_2}^n - \tilde{\rho}_{1,h_1}^n\right), \xi_{h_2}\right) &= 0.\end{aligned} \tag{A.1}$$

Next, for $\tilde{k}_2 \not\equiv 0$, as in [26] we define the elliptic projection $\langle P\tilde{\rho}_1, P\tilde{\rho}_2 \rangle$ of $\langle \tilde{\rho}_1, \tilde{\rho}_2 \rangle$ into $V_{h_1} \times V_{h_2}$ via

$$\left(\nabla\left(P\tilde{\rho}_i - \tilde{\rho}_i\right), \nabla \chi\right) = 0, \quad \forall \chi \in V_{h_i},\ i = 1, 2. \tag{A.2}$$

Applying (A.2) for $i = 1, 2$ into the weak formulation (2.4), with arbitrary $\psi, \xi \in H_D^1(\Omega)$ we arrive at

$$\begin{aligned}\left(\tilde{\phi}_1 \frac{\partial P\tilde{\rho}_1}{\partial t}, \psi\right) + \left(\tilde{k}_1 \nabla P\tilde{\rho}_1, \nabla \psi\right) + \left(c(\tilde{\rho}_1 - \tilde{\rho}_2), \psi\right) &= (f, \psi) + \left(\tilde{\phi}_1 \frac{\partial\left(P\tilde{\rho}_1 - \tilde{\rho}_1\right)}{\partial t}, \psi\right),\\ \left(\tilde{\phi}_2 \frac{\partial P\tilde{\rho}_2}{\partial t}, \xi\right) + \left(\tilde{k}_2 \nabla P\tilde{\rho}_2, \nabla \xi\right) + \left(c(\tilde{\rho}_2 - \tilde{\rho}_1), \xi\right) &= \left(\tilde{\phi}_2 \frac{\partial\left(P\tilde{\rho}_2 - \tilde{\rho}_2\right)}{\partial t}, \xi\right).\end{aligned} \tag{A.3}$$

Next we define $\partial^n w = (w(t_n) - w(t_{n-1}))/\Delta t_n$, $\Delta_n(w) = \partial^n w - (\partial w/\partial t)(t_n)$, subtract (A.3) from (A.1), add the resulting equations, and use as test functions $\psi = \tilde{\rho}^n_{1,h_1} - P\tilde{\rho}^n_1$ and $\xi = \tilde{\rho}^n_{2,h_2} - P\tilde{\rho}^n_2$ to get

$$\begin{aligned}
&\tilde{\phi}_1\left\|\tilde{\rho}^n_{1,h_1} - P\tilde{\rho}^n_1\right\|^2 + \tilde{\phi}_2\left\|\tilde{\rho}^n_{2,h_2} - P\tilde{\rho}^n_2\right\|^2 + \tilde{k}_1\Delta t_n\left|\tilde{\rho}^n_{1,h_1} - P\tilde{\rho}^n_1\right|_1^2 + \tilde{k}_2\Delta t_n\left|\tilde{\rho}^n_{2,h_2} - P\tilde{\rho}^n_2\right|_1^2 \\
&\quad\le \tilde{\phi}_1\left(\tilde{\rho}^{n-1}_{1,h_1} - P\tilde{\rho}^{n-1}_1, \tilde{\rho}^n_{1,h_1} - P\tilde{\rho}^n_1\right) + \tilde{\phi}_2\left(\tilde{\rho}^{n-1}_{2,h_2} - P\tilde{\rho}^{n-1}_2, \tilde{\rho}^n_{2,h_2} - P\tilde{\rho}^n_2\right) \\
&\qquad + \Delta t_n\left(\tilde{\phi}_1\frac{\partial(P\tilde{\rho}_1 - \tilde{\rho}_1)}{\partial t}, \tilde{\rho}^n_{1,h_1} - P\tilde{\rho}^n_1\right) + \Delta t_n\left(\tilde{\phi}_2\frac{\partial(P\tilde{\rho}_2 - \tilde{\rho}_2)}{\partial t}, \tilde{\rho}^n_{2,h_2} - P\tilde{\rho}^n_2\right) \\
&\qquad - \Delta t_n\left(\tilde{\phi}_1\Delta_n(P\tilde{\rho}_1), \tilde{\rho}^n_{1,h_1} - P\tilde{\rho}^n_1\right) - \Delta t_n\left(\tilde{\phi}_2\Delta_n(P\tilde{\rho}_2), \tilde{\rho}^n_{2,h_2} - P\tilde{\rho}^n_2\right).
\end{aligned} \tag{A.4}$$

With the help of standard inequalities, summing the equations from $n = 1\ldots, N$, and applying the discrete Gronwall's lemma with $\beta = 2\max\{\tilde{\phi}_1, \tilde{\phi}_2\}$, we get

$$\begin{aligned}
\left|\left\|\left\langle\tilde{\rho}^n_{1,h_1} - P\tilde{\rho}^n_1, \tilde{\rho}^n_{2,h_2} - P\tilde{\rho}^n_2\right\rangle\right\|\right|^2 \le e^{\beta t_N}\Bigg\{&\tilde{\phi}_1\left\|\tilde{\rho}^0_{1,h_1} - P\tilde{\rho}^0_1\right\|^2 + \tilde{\phi}_2\left\|\tilde{\rho}^0_{2,h_2} - P\tilde{\rho}^0_2\right\|^2 \\
&+ \sum_{n=1}^{N}\Delta t_n\tilde{\phi}_1\left(\left\|\frac{\partial(P\tilde{\rho}_1 - \tilde{\rho}_1)}{\partial t}\right\|^2 + \left\|\Delta_n(P\tilde{\rho}_1)\right\|^2\right) \\
&+ \sum_{n=1}^{N}\Delta t_n\tilde{\phi}_2\left(\left\|\frac{\partial(P\tilde{\rho}_2 - \tilde{\rho}_2)}{\partial t}\right\|^2 + \left\|\Delta_n(P\tilde{\rho}_2)\right\|^2\right)\Bigg\}.
\end{aligned} \tag{A.5}$$

Next step is to estimate the quantities $\|\partial(P\tilde{\rho}_i - \tilde{\rho}_i)/\partial t\|$, $\|\Delta_n(P\tilde{\rho}_i)\|$, $i = 1, 2$. This is done using standard properties of elliptic projections as in [25, Lemmas 13.2 and 13.4, pages 233 and 241] assuming $\tilde{\rho}_i, \partial\tilde{\rho}_i/\partial t$ are smooth enough. Combining these we arrive at the desired inequality (4.5).

For the case $\tilde{k}_2 \equiv 0$, we define $P^*\tilde{\rho}_2$ as the L^2-projection of $\tilde{\rho}_2$ over $V^n_{h_2}$ via

$$(P^*\tilde{\rho}_2 - \tilde{\rho}_2, \chi) = 0 \quad \forall\chi \in V^n_{h_2}. \tag{A.6}$$

The proof follows along the same lines as for $\tilde{k}_2 \not\equiv 0$ except that we do not (and cannot) use any terms with $\nabla\tilde{\rho}_2$. □

B. Proof of Theorem 4.2

Proof. The proof is a combination of techniques in [13–15] which we extend to a coupled system and propose an estimator robust with respect to the five parameters of the problem.

First we define the semidiscrete problem: find $\{\langle\tilde{\rho}_1^n,\tilde{\rho}_2^n\rangle\}_{n=1}^N \in (H_D^1(\Omega))^2$ so that for all $\langle\psi,\xi\rangle \in (H_D^1(\Omega))^2$

$$\begin{aligned}\left(\tilde{\phi}_1\tilde{\rho}_1^n,\psi\right)+\left(\tilde{k}_1\nabla\tilde{\rho}_1^n,\nabla\psi\right)+\left(c(\tilde{\rho}_1^n-\tilde{\rho}_2^n),\psi\right)&=(f,\psi)+\left(\tilde{\phi}_1\tilde{\rho}_1^{n-1},\psi\right),\\ \left(\tilde{\phi}_2\tilde{\rho}_2^n,\xi\right)+\left(\tilde{k}_2\nabla\tilde{\rho}_2^n,\nabla\xi\right)+\left(c(\tilde{\rho}_2^n-\tilde{\rho}_1^n),\xi\right)&=\left(\tilde{\phi}_2\tilde{\rho}_2^{n-1},\xi\right).\end{aligned}\tag{B.1}$$

We estimate the error between the solution of (2.4) and (B.1) and this is how the time estimator T^n (4.7) arises; see [15] for details.

Now the semidiscrete system (B.1) is a stationary coupled reaction-diffusion model of a type we considered in [13] and for which we proposed a spatial a posteriori error estimator accounting for the coupling terms in the system. That estimator is robust, that is, the efficiency ratio remains essentially constant when the coefficients change by orders of magnitude; this is relevant for our problem since we may have small $\tilde{k}_2$. The robustness in [13] is achieved by an appropriate scaling of constants in the estimator; the scaling in (4.11)–(4.13) serves the same purpose.

Recall the standard set-up first. Fix $i = 1, 2$, and for any $T \in \mathcal{T}_{h_i}^n$ denote by $\tilde{\omega}_T$ the set of all elements in $\mathcal{T}_{h_i}^n$ that share at least one vertex with T. For the quasi-interpolator Q_h defined in [14, Lemma 3.1, page 482], we have that for any $v \in H^k(\tilde{\omega}_T)$, $0 \le k \le 1$,

$$\left\|\nabla^l(v-Q_hv)\right\|_T \le Ch_T^{k-l}\left\|\nabla^k v\right\|_{\tilde{\omega}_T} \quad 0\le l\le k\le 1,\tag{B.2}$$

where the constant C is independent of h, v, and where $\nabla^0 v = v$. The plan is to extend (B.2) for $l = 0$ to an inequality involving the form

$$\mathcal{B}_T=\left(\int_{\tilde{\omega}_T} c(\xi-\psi)^2+\tilde{k}_2(\nabla\psi)^2+\tilde{k}_1(\nabla\xi)^2\right)^{1/2},\tag{B.3}$$

which involves the coupling term as well as other coefficients of the problem and thus leads to robustness.

If $\tilde{k}_2 > 0$, let $\xi, \psi \in H^1(\Omega)$ and recall that $V_{h_2}^n \subseteq V_{h_1}^n$. If $\tilde{k}_2 \equiv 0$, we consider $\xi \in H_D^1(\Omega)$, $\psi \in L^2(\Omega)$, and away from the boundary on some $\overset{\circ}{\Omega} \subsetneq \Omega$ we have $V_{h_2}^n(\overset{\circ}{\Omega}) \subseteq V_{h_1}^n(\overset{\circ}{\Omega})$. For a fixed n, i, let ξ_{h_i}, ψ_{h_i} be the quasi-interpolators of ϕ, ψ in $V_{h_i}^n$, respectively. Note that ψ_{h_2} is defined correctly when $k_2 = 0$ and $\psi \in L^2(\Omega)$. To get the desired estimate, we apply (B.2) with $T \in \mathcal{T}_{h_1}^n$, and $l = 0$, $k = 1$, to get $\|\xi-\xi_{h_1}\|_T \le h_T\|\nabla\xi\|_{\tilde{\omega}_T}\xi\|_{\tilde{\omega}_T} \le (h_T/\tilde{k}_1^{1/2})\mathcal{B}_T$. To extend, we add and subtract $\psi - \psi_{h_1}$ and use the triangle inequality followed by (B.2) with $k = l = 0$ and $k = 1$, $l = 0$ to get

$$\begin{aligned}\|\xi-\xi_{h_1}\|_T &\le \left\|(\xi-\xi_{h_1})-(\psi-\psi_{h_1})\right\|_T+\left\|\psi-\psi_{h_1}\right\|_T\\ &\le \left\|\xi-\psi\right\|_{\tilde{\omega}_T}+h_T\left\|\nabla\psi\right\|_{\tilde{\omega}_T}\le\sqrt{2}\max\left\{\frac{1}{c^{1/2}},\frac{h_T}{\tilde{k}_2^{1/2}}\right\}\mathcal{B}_T.\end{aligned}\tag{B.4}$$

Thus we have by (4.11)

$$\|\xi - \xi_{h_1}\|_T \leq \theta_{1,T}\mathcal{B}_T, \tag{B.5}$$

which is the desired element estimate.

To prove the edge interpolation estimate for an edge E of the element T, we use the following trace inequality [43, Lemma 3.1, page 645] for $v \in H^1(T)$:

$$\|v\|_E \leq C\left(h_T^{-1/2}\|v\|_T + \|v\|_T^{1/2}\|\nabla v\|_T^{1/2}\right), \tag{B.6}$$

where C is a constant independent of v, h_T. Let $v = \xi - \xi_{h_1}$. By (B.2)

$$\|\nabla(\xi - \xi_{h_1})\|_T \leq \|\nabla\xi\|_{\tilde{\omega}_T} \leq h_T^{-1}\theta_{1,T}\mathcal{B}_T. \tag{B.7}$$

Applying (B.6) followed by (B.5) and (B.7) we get

$$\begin{aligned}\|\xi - \xi_{h_1}\|_E &\leq h_T^{-1/2}\|\xi - \xi_{h_1}\|_T + \|\xi - \xi_{h_1}\|_T^{1/2}\|\nabla\xi - \xi_{h_1}\|^{1/2} \\ &\leq h_T^{-1/2}\theta_{1,T}\mathcal{B}_T + \theta_{1,T}^{1/2}\mathcal{B}_T^{1/2}h_T^{-1/2}\theta_{1,T}^{1/2}\mathcal{B}_T^{1/2}.\end{aligned} \tag{B.8}$$

Thus we obtain $\|\xi - \xi_{h_1}\|_E \leq \gamma_{1,E}\mathcal{B}_T$, and the estimate for the second component follows similarly if $\tilde{k}_2 \not\equiv 0$.

When $\tilde{k}_2 \equiv 0$, we have $\xi \in H_D^1(\Omega)$, $\psi \in L^2(\Omega)$, and (4.12) is reduced to $\theta_{2,T} = \max\{1/c^{1/2}, h_T/\tilde{k}_1^{1/2}\}$. Also, $\gamma_{2,T}$ does not need to be defined since $R_{2,E}^n \equiv 0$. Now we add and subtract $\psi - \psi_{h_1}$ and use the triangle inequality followed by (B.2) with $k = l = 0$ and $k = 1, l = 0$ to get

$$\begin{aligned}\|\psi - \psi_{h_2}\|_T &\leq \|(\xi - \xi_{h_1}) - (\psi - \psi_{h_1})\|_T + \|\xi - \xi_{h_1}\|_T \\ &\leq \|\xi - \psi\|_{\tilde{\omega}_T} + h_T\|\nabla\xi\|_{\tilde{\omega}_T} \leq \sqrt{2}\max\left\{\frac{1}{c^{1/2}}, \frac{h_T}{\tilde{k}_1^{1/2}}\right\}\mathcal{B}_T.\end{aligned} \tag{B.9}$$

Thus, by (4.12) we have $\|\psi - \psi_{h_1}\|_T \leq \theta_{2,T}\mathcal{B}_T$, which is the desired edge estimate.

Combining these interpolation estimates with the usual technique of upper bounds for residual a posteriori error estimators extended to systems in [13] completes the proof the theorem. □

Acknowledgments

The authors would like to thank Professor Ralph Showalter from Oregon State University for numerous discussions on the double-diffusion models. they would like also to acknowledge the package *i*FEM [44] which was used to refine and coarsen the grid in our adaptive implementation. they are also grateful to the anonymous referee whose remarks helped to improve the paper. This work was partially supported by the Grants NSF DMS-0511190, DMS-1115827, DOE 98089, and by FAPESP/Brazil.

References

[1] A. Bensoussan, J.-L. Lions, and G. Papanicolaou, *Asymptotic Analysis for Periodic Structures*, vol. 5 of *Studies in Mathematics and Its Applications*, North-Holland, Amsterdam, The Netherlands, 1978.

[2] E. Sánchez-Palencia, *Nonhomogeneous Media and Vibration Theory*, vol. 127 of *Lecture Notes in Physics*, Springer, Berlin, Germany, 1980.

[3] U. Hornung, Ed., *Homogenization and Porous Media*, vol. 6 of *Interdisciplinary Applied Mathematics*, Springer, New York, NY, USA, 1997.

[4] G. I. Barenblatt, Iu. P. Zheltov, and I. N. Kochina, "Basic concepts in the theory of seepage of homogeneous liquids in fissured rocks [strata]," *Journal of Applied Mathematics and Mechanics*, vol. 24, no. 5, pp. 1286–1303, 1960.

[5] L. I. Rubinšteĭn, "On a question about the propagation of heat in heterogeneous media," vol. 12, pp. 27–45, 1948.

[6] J. E. Warren and P. J. Root, "The behavior of naturally fractured resevoirs," *Society of Petroleum Engineers Journal*, vol. 3, pp. 245–255, 1963.

[7] E. Ruckenstein, A. S. Vaidyanathan, and G. R. Youngquist, "Sorption by solids with bidisperse pore structures," *Chemical Engineering Science*, vol. 26, no. 9, pp. 1305–1318, 1971.

[8] G. R. King, T. Ertekin, and F. C. Schwerer, "Numerical simulation of the transient behavior of coal-seam degasification wells," *SPE Formation Evaluation*, vol. 1, no. 2, pp. 165–183, 1986.

[9] J. Q. Shi and S. Durucan, "A bidisperse pore diffusion model for methane displacement desorption in coal by CO_2 injection," *Fuel*, vol. 82, no. 10, pp. 1219–1229, 2003.

[10] J.-Q. Shi, S. Mazumder, K.-H. Wolf, and S. Durucan, "Competitive methane desorption by supercritical CO_2 injection in coal," *Transport in Porous Media*, vol. 75, no. 1, pp. 35–54, 2008.

[11] R. E. Showalter and D. B. Visarraga, "Double-diffusion models from a highly-heterogeneous medium," *Journal of Mathematical Analysis and Applications*, vol. 295, no. 1, pp. 191–210, 2004.

[12] T. Arbogast, J. Douglas Jr., and U. Hornung, "Derivation of the double porosity model of single phase flow via homogenization theory," *SIAM Journal on Mathematical Analysis*, vol. 21, no. 4, pp. 823–836, 1990.

[13] V. Klein and M. Peszyńska, "Robust a-posteriori estimators for multilevel discretizations of reaction-diffusion systems," *IJNAM*, vol. 8, no. 1, pp. 1–27, 2011.

[14] R. Verfürth, "Robust a posteriori error estimators for a singularly perturbed reaction-diffusion equation," *Numerische Mathematik*, vol. 78, no. 3, pp. 479–493, 1998.

[15] A. Bergam, C. Bernardi, and Z. Mghazli, "A posteriori analysis of the finite element discretization of some parabolic equations," *Mathematics of Computation*, vol. 74, no. 251, pp. 1117–1138, 2005.

[16] G. Sangalli, "Robust a-posteriori estimator for advection-diffusion-reaction problems," *Mathematics of Computation*, vol. 77, no. 261, pp. 41–70, 2008.

[17] L. C. Evans, *Partial Differential Equations*, vol. 19 of *Graduate Studies in Mathematics*, American Mathematical Society, Providence, RI, USA, 1998.

[18] R. E. Showalter, *Hilbert Space Methods for Partial Differential Equations*, Pitman, London, UK, 1977.

[19] T. Arbogast, "Analysis of the simulation of single phase flow through a naturally fractured reservoir," *SIAM Journal on Numerical Analysis*, vol. 26, no. 1, pp. 12–29, 1989.

[20] A. Quarteroni and A. Valli, *Numerical Approximation of Partial Differential Equations*, vol. 23 of *Springer Series in Computational Mathematics*, Springer, Berlin, Germany, 1997.

[21] E. C. Aifantis and J. M. Hill, "On the theory of diffusion in media with double diffusivity. I. Basic mathematical results," *The Quarterly Journal of Mechanics and Applied Mathematics*, vol. 33, no. 1, pp. 1–21, 1980.

[22] J. M. Hill and E. C. Aifantis, "On the theory of diffusion in media with double diffusivity. II. Boundary-value problems," *The Quarterly Journal of Mechanics and Applied Mathematics*, vol. 33, no. 1, pp. 23–41, 1980.

[23] R. Verfürth, *A Review of a Posteriori Error Estimation and Adaptive Mesh-Refinement Techniques*, Wiley & Teubner, 1996.

[24] D. Braess, *Finite Elements*, Cambridge University Press, Cambridge, UK, 3rd edition, 2007.

[25] V. Thomée, *Galerkin Finite Element Methods for Parabolic Problems*, vol. 25 of *Springer Series in Computational Mathematics*, Springer, Berlin, Germany, 2nd edition, 2006.

[26] M. F. Wheeler, "A priori L_2 error estimates for Galerkin approximations to parabolic partial differential equations," *SIAM Journal on Numerical Analysis*, vol. 10, pp. 723–759, 1973.

[27] K. Eriksson and C. Johnson, "Adaptive finite element methods for parabolic problems. II. Optimal error estimates in $L_\infty L_2$ and $L_\infty L_\infty$," *SIAM Journal on Numerical Analysis*, vol. 32, no. 3, pp. 706–740, 1995.

[28] M. Picasso, "Adaptive finite elements for a linear parabolic problem," *Computer Methods in Applied Mechanics and Engineering*, vol. 167, no. 3-4, pp. 223–237, 1998.

[29] R. Verfürth, "A posteriori error estimates for finite element discretizations of the heat equation," *Calcolo*, vol. 40, no. 3, pp. 195–212, 2003.

[30] L. J. Durlofsky, "Numerical calculation of equivalent grid block permeability tensors for heterogeneous porous media," *Water Resources Research*, vol. 27, no. 5, pp. 699–708, 1991.

[31] R. E. Showalter and N. J. Walkington, "Elliptic systems for a medium with microstructure," in *Geometric Analysis and Nonlinear Partial Differential Equations*, vol. 144 of *Lecture Notes in Pure and Applied Mathematics*, pp. 91–104, Dekker, New York, NY, USA, 1993.

[32] M. Peszyńska, "Analysis of an integro-differential equation arising from modelling of flows with fading memory through fissured media," *Journal of Partial Differential Equations*, vol. 8, no. 2, pp. 159–173, 1995.

[33] M. Peszyńska, "Finite element approximation of diffusion equations with convolution terms," *Mathematics of Computation*, vol. 65, no. 215, pp. 1019–1037, 1996.

[34] J. Douglas Jr., M. Peszyńska, and R. E. Showalter, "Single phase flow in partially fissured media," *Transport in Porous Media*, vol. 28, no. 3, pp. 285–306, 1997.

[35] M. Peszyńska and R. E. Showalter, "Multiscale elliptic-parabolic systems for flow and transport," *Electronic Journal of Differential Equations*, no. 147, 30 pages, 2007.

[36] G. F. Carey, S.-S. Chow, and M. K. Seager, "Approximate boundary-flux calculations," *Computer Methods in Applied Mechanics and Engineering*, vol. 50, no. 2, pp. 107–120, 1985.

[37] J. Xu, "Two-grid discretization techniques for linear and nonlinear PDEs," *SIAM Journal on Numerical Analysis*, vol. 33, no. 5, pp. 1759–1777, 1996.

[38] C. N. Dawson and M. F. Wheeler, "Two-grid methods for mixed finite element approximations of nonlinear parabolic equations," in *Domain Decomposition Methods in Scientific and Engineering Computing*, vol. 180 of *Contemporary Mathematics*, pp. 191–203, American Mathematical Society, Providence, RI, USA, 1994.

[39] V. Klein and M. Peszynska, "Adaptive multi-level modeling of coupled multiscale phenomena with applications to methane evolution in subsurface," in *Proceedings of the 18th International Conference on Computational Methods in Water Resources (CMWR '11)*, Barcelona, Spain, June 2001.

[40] V. Klein, *Two-grid a-priori and a-posteriori error analysis for coupled elliptic and parabolic systems with applications to flow and transport equations [Ph.D. thesis]*, Oregon State University, 2011.

[41] P. Morin, K. G. Siebert, and A. Veeser, "A basic convergence result for conforming adaptive finite elements," *Mathematical Models & Methods in Applied Sciences*, vol. 18, no. 5, pp. 707–737, 2008.

[42] R. Verfürth, "Robust a posteriori error estimates for nonstationary convection-diffusion equations," *SIAM Journal on Numerical Analysis*, vol. 43, no. 4, pp. 1783–1802, 2005.

[43] R. Verfürth, "A posteriori error estimators for convection-diffusion equations," *Numerische Mathematik*, vol. 80, no. 4, pp. 641–663, 1998.

[44] L. Chen, "Short implementation of bisection in MATLAB," in *Recent Advances in Computational Sciences*, pp. 318–332, World Scientific, Hackensack, NJ, USA, 2008.

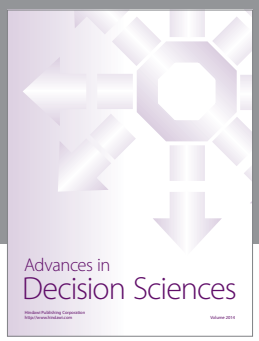

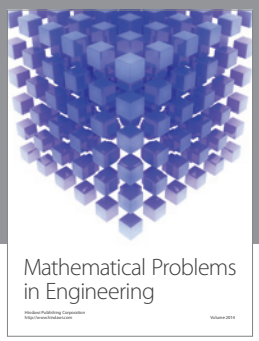

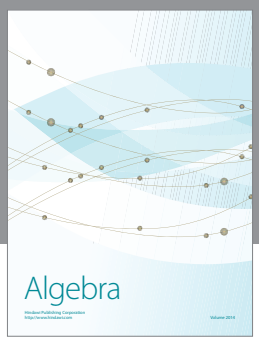

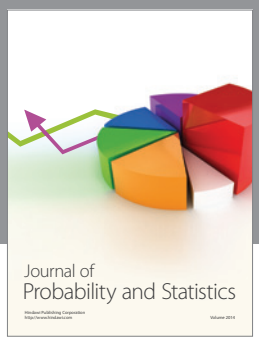

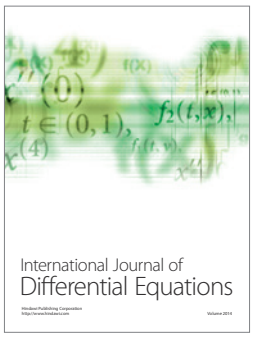

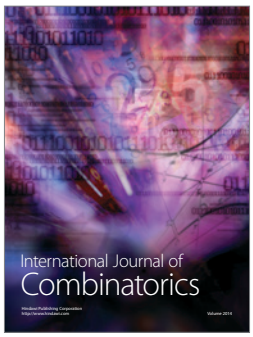

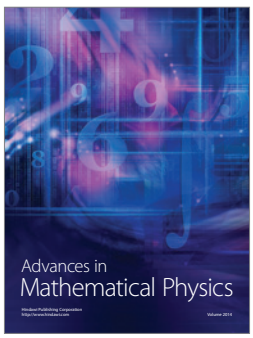

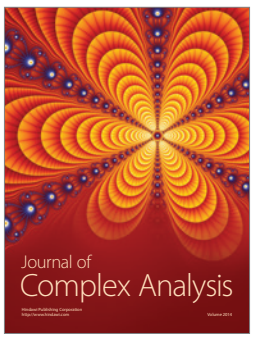

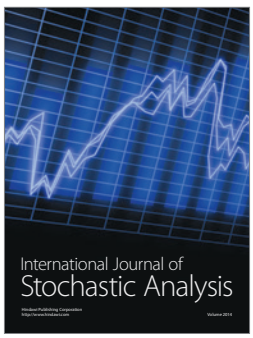

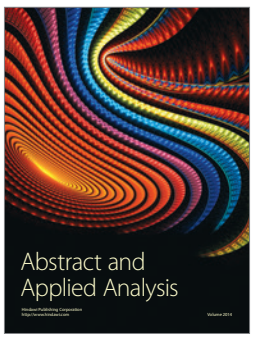

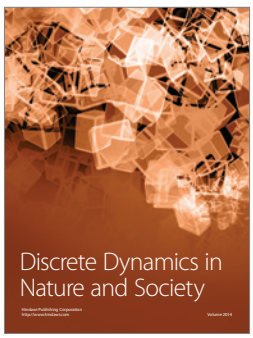

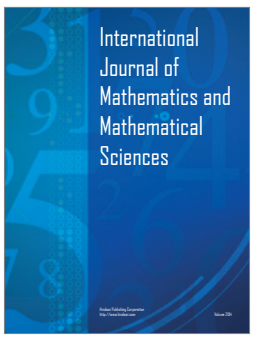

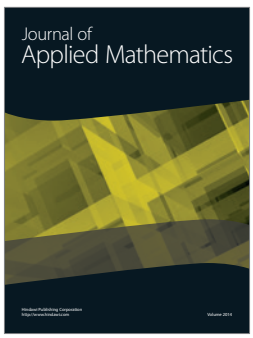

Hindawi
Submit your manuscripts at
http://www.hindawi.com